Cell Reports
Physical Science

CellPress
OPEN ACCESS

Review

Structure and applications of PIC-based polymers and hydrogels

Kaizheng Liu,[1,2,3,9] Johannes Vandaele,[2,9] Hongbo Yuan,[2,4] Kerstin G. Blank,[5,6] Roel Hammink,[2,7,8,*] Paul H.J. Kouwer,[3,*] and Susana Rocha[2,*]

SUMMARY

Over the last decade, water-soluble polyisocyanopeptides (PICs) have emerged as a new class of biomimetic polymers. Analogous to biopolymers, PICs exhibit a semi-flexible nature; however, unlike their biological counterparts, they possess the unique advantage of being highly customizable. Hydrogels made of PICs have a fibrous and porous architecture and, consequently, unique mechanical properties. This includes strain stiffening, which is well known in biological materials but rarely found in synthetic gels. These properties make PIC hydrogels uniquely suited for a wide range of biological applications. One key application is their use as a highly tailorable, biomimetic 3D cell culture matrix, which also allows for investigating interactions between cells and their environment. Beyond gel applications, soluble PICs are used in an immunological setting, where they provide a multivalent scaffold for the development of synthetic dendritic cells. This review aims to provide a comprehensive overview of PICs, encompassing their structure, properties, and key applications. First, we discuss the history, synthesis, and characterization methods of PIC hydrogels, followed by an overview of current applications that range from biosensing and immunotherapy to cell culture and wound healing. Presenting these different applications, we demonstrate that these polymers are a multi-versatile scaffold, triggering the interest of material scientists, biologists, chemists, and medical engineers.

POLYISOCYANIDES: HISTORY, SYNTHESIS, AND FUNCTIONALIZATION

Polyisocyanides are obtained by the polymerization of isocyanides. Although discovered late in the 1850s,[1] it took almost a full century until Ugi and Meyr introduced a straightforward protocol for the synthesis of polyisocyanides.[2] In 1972, a catalyst-based polymerization reaction with acid-coated glass was introduced.[3] Later, methods based on metal complex catalysts were introduced,[4–6] for instance, using Ni(II) salts. This method gives the polymers a unique secondary structure.[7,8] The polymerization reaction proceeds via a "merry-go-round" mechanism and yields a helical backbone with approximately four monomers per turn (4_1 helix).[9,10] This mechanism is initiated by the formation of a tetrakis(isocyanide) Ni(II) complex, which is activated by the addition of a nucleophile, most typically an amine or an alcohol (Figure 1).[9] We note that polymers with helical conformations are prevalent in nature where they are typically used as structural features.[11] As such, the development of helical synthetic polymers such as PIC is a milestone in engineering life-like materials.

[1]Research Center for Human Tissues and Organs Degeneration, Institute of Biomedicine and Biotechnology, Shenzhen Institute of Advanced Technology, Chinese Academy of Sciences, Shenzhen 518055, China

[2]Molecular Imaging and Photonics, Chemistry Department, KU Leuven, 3000 Leuven, Belgium

[3]Institute for Molecules and Materials, Radboud University, 6525 AJ Nijmegen, the Netherlands

[4]Key Laboratory of Molecular Biophysics of Hebei Province, Institute of Biophysics, School of Health Sciences and Biomedical Engineering, Hebei University of Technology, Tianjin 300401, China

[5]Mechano(bio)chemistry, Max Planck Institute of Colloids and Interfaces, Am Mühlenberg 1, 14476 Potsdam, Germany

[6]Department of Biomolecular and Selforganizing Matter, Institute of Experimental Physics, Johannes Kepler University, Altenberger Str. 69, 4040 Linz, Austria

[7]Department of Medical BioSciences, Radboud University Medical Center, Geert Grooteplein 26, 6525 GA Nijmegen, the Netherlands

[8]Division of Immunotherapy, Oncode Institute, Radboud University Medical Center, Geert Grooteplein 26, 6525 GA Nijmegen, the Netherlands

[9]These authors contributed equally

*Correspondence:
roel.hammink@radboudumc.nl (R.H.),
paul.kouwer@ru.nl (P.H.J.K.),
susana.rocha@kuleuven.be (S.R.)

https://doi.org/10.1016/j.xcrp.2024.101834

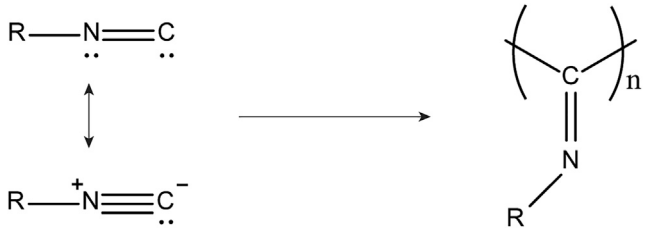

Figure 1. Polymerization of isocyanides to yield a polyisocyanide polymer
Adapted from Cornelissen et al.[10]

All carbon atoms in the polyisocyanide backbone bear a substituent. Neighboring substituents feel steric hindrance, forcing the polymer backbone to retain the helical conformation.[10] Bulky groups in the side chain lock the backbone conformation, which results in preservation of the helical sense.[7] If the side chains are not bulky enough, however, the polymer is more dynamic and conformational changes are possible.[12,13]

Alternatively, the helical structure can be preserved by the incorporation of stabilizing hydrogen-bonding networks in the side chains of the polymer. This strategy has been elegantly implemented by synthesizing polyisocyanides with di- or tripeptide functionalized side chains, so-called polyisocyanopeptides (PICs).[14–16] Using these short peptide side chains, hydrogen bonding occurs between the amide bonds of parallel side chains, i.e., between side chains n and $n + 4$.[14] The distance between the participating amide bonds was estimated to be 0.46 nm and an overall β sheet-like packing of the side chains was found along the polymer backbone.[14] As a result of this interaction, very long (from 100 nm to several micrometers) and relatively rigid polymers were formed. The stiffness of a given polymer is quantified using its persistence length, i.e., the length where the correlation of angles of the tangent vector is lost; higher persistence lengths correspond to stiffer polymers.[17] PIC polymers have a persistence length up to 76 nm.[18] As this value is similar to their contour length, PICs are classified as semi-flexible polymers. The high degree of polymerization, combined with the highly defined backbone structure and stiffness make PICs ideal polymers to organize electroactive and optically active (chromophoric) groups in array-like arrangements. Over the years, many examples have been published[19,20] but we will focus on polymers with water-soluble substituents that allows us to enter the biological context.

WATER-SOLUBLE POLYISOCYANOPEPTIDES

Drawing inspiration from well-defined biopolymers, research focused on the synthesis of water-soluble PICs. As the polymerization is poorly compatible with protic solvents, different strategies were followed to obtain water solubility. In a first attempt, post-polymerization modifications were introduced by (co)polymerizing an isocyano-*D*-alanyl-*L*-alanine methyl ester monomer.[21] Upon saponification (hydrolysis of the methyl ester, Figure 2A), and subsequent generation of negatively charged carboxylic acid groups, this polymer became water soluble. In an alternative approach, water solubility was achieved by a different post-modification approach: acetylene-bearing homopolymers were reacted with azide-functionalized OEG side chains (Figure 2B).[22] The polymer obtained was water soluble but the addition of the OEG side chains using this approach induced a change in the circular dichroism (CD) spectrum, which could point toward a partial unfolding of the polymer or indicate that the polymer acquires another helical state,

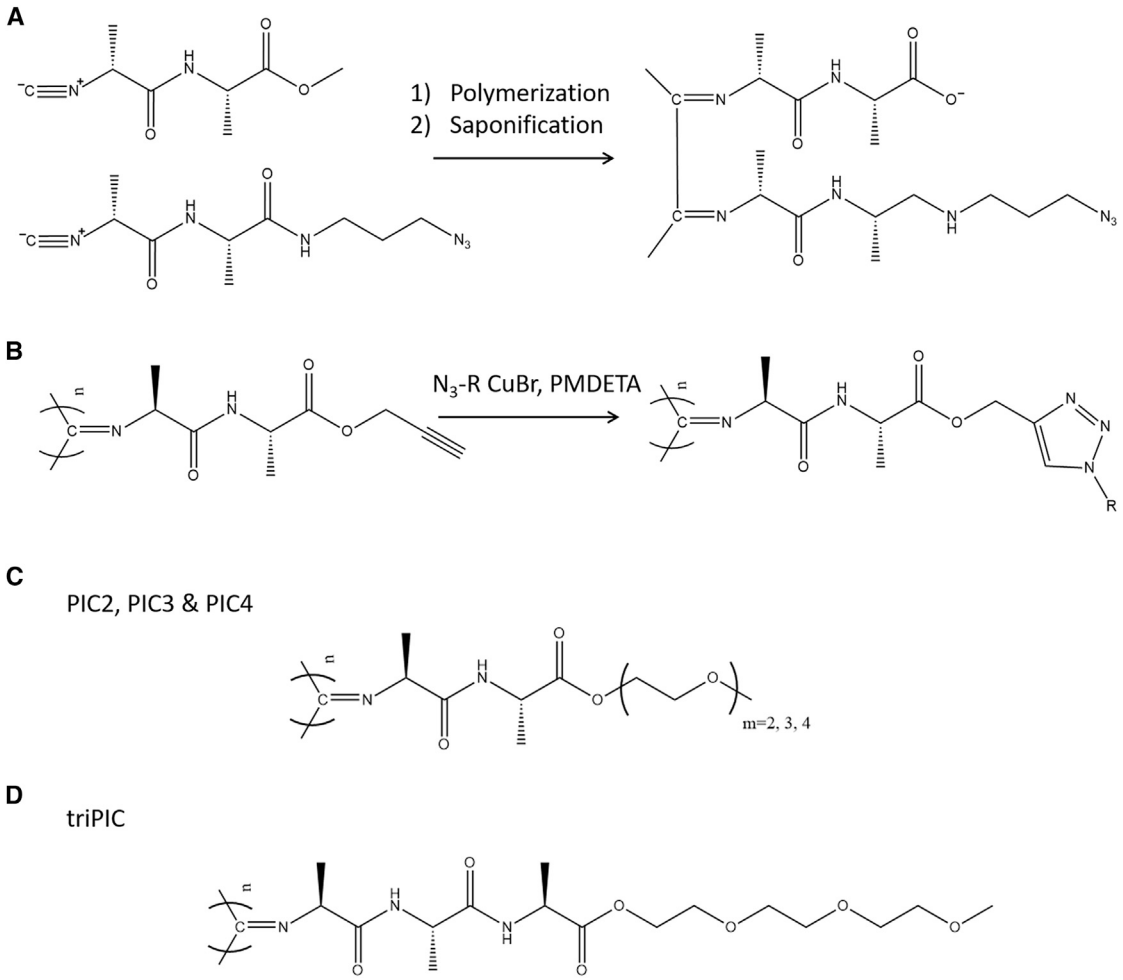

Figure 2. Strategies to obtain water-soluble PICs

(A) Azide-functionalized monomers are polymerized with methyl ester-containing monomers, yielding a statistical distribution of functional monomers in the polymer backbone. Saponification of the methyl ester results in a water-soluble polymer. Adapted from Schwartz et al.[21]

(B) Acetylene-functionalized PICs able to react with azides in a copper-catalyzed azide-alkyne cycloaddition reaction with R = OEG. Adapted from Kitto et al.[22]

(C) PICs with side chains bearing two (PIC2), three (PIC3), or four (PIC4) ethylene glycol units. Reprinted from Koepf et al.[23]

(D) PICs with side chains consisting of three ethylene glycol units and three amino acids (*L-D-L* alanine). Reprinted from Yuan et al.[27]

characterized by a different chain arrangement. To circumvent the intrinsic disadvantages of post-modification reactions (conversion, side reactions, conformational changes, etc.), the direct polymerization of OEG-containing isocyanopeptide monomers was investigated, containing two, three, or four ethylene glycol units (Figure 2C).[23]

Further research focused on synthetic routes from an isocyanopeptide monomer already equipped with the oligo(ethylene glycol) tail. These polymerization reactions are readily carried out in toluene,[23] where low initiator concentrations lead to high-molecular-weight polymers (> 500 kDa) with polydispersities around 1.3–1.4. This value has been estimated from the results of viscometry and atomic force microscopy (AFM) experiments.[24] The length of the glycol tail has large effects on the physiochemical properties of the polymers; PICs bearing a tail containing two ethylene glycol units do not dissolve in water. In contrast, good water solubility was

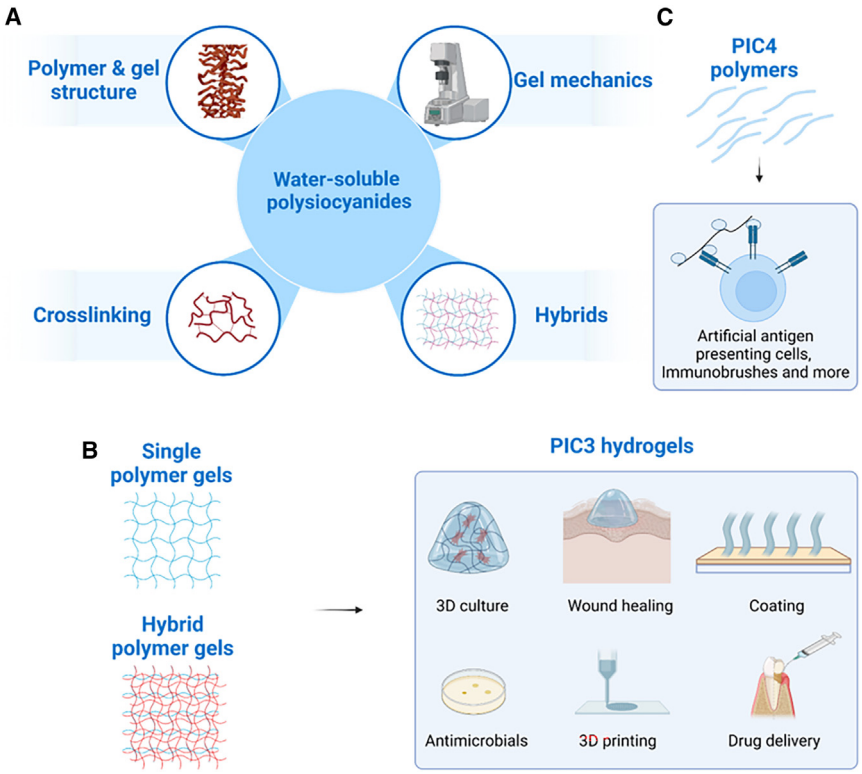

Figure 3. Overview of the properties and applications of water-soluble polyisocyanopeptides
(A) Key properties of polyisocyanopeptide (PIC) polymers and hydrogels, including methods for tuning gel mechanics.
(B and C) Structure and applications of PIC3 hydrogels (B) and PIC4 polymers (C). The figure was created with BioRender.

observed for the polymers possessing three (PIC3) or four (PIC4) ethylene glycol units in their side chains. Interestingly, PICs functionalized with 3OEG and 4OEG showed thermo-responsive behavior in aqueous solutions. When the temperature of these PIC solutions was increased above the lower critical solution temperature (LCST), the polymers did not precipitate, but rather formed a mechanically stable gel, even at ultra-low concentrations down to 0.006 wt %.[25] The properties of these materials are discussed in detail in the following sections.

The obtained water-soluble polymers can readily be further modified by introducing functional groups into the OEG side chains. One strategy is to generate a library of monomers that contain all desired functional groups; however, this requires a large synthetic effort and the optimization of polymerization conditions per monomer mixture. This strategy is also limited to functional groups that are compatible with the Ni^{2+}-catalyzed polymerization reaction.[26] Alternatively, a two-step process is commonly used. In the polymerization reaction, a monomer carrying an azide moiety is used together with a non-functionalized monomer to yield a copolymer with a defined density of azide moieties. After polymerization and purification, different functional groups are then grafted to the polymer using the efficient strain-promoted azide-alkyne cycloaddition (SPAAC) reaction. As discussed in more detail later, this method has been used to introduce fluorescent labels, oligonucleotides, peptides, and antibodies, among other moieties, rendering multifunctional polymers and hydrogels (Figure 3).

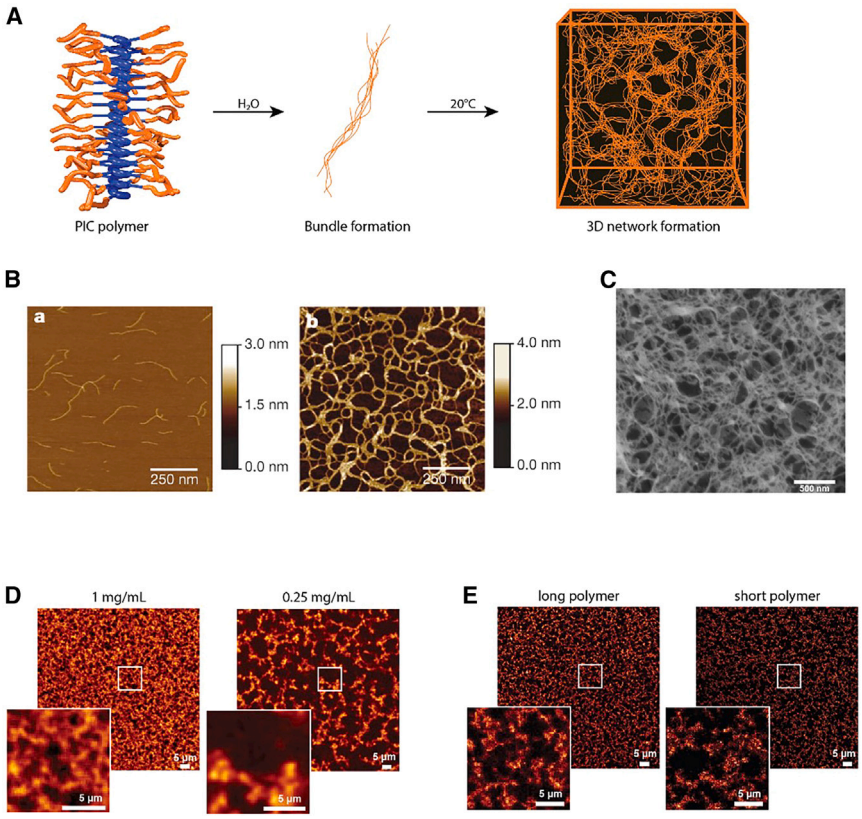

Figure 4. Structural characterization of PIC3 hydrogels

(A) Schematic representation of the gelation mechanism of the PIC3 polymer. In water, the PIC3 polymer dissolves and upon heating the solution above 20°C–25°C a hydrogel network is formed.

(B) Left: AFM-image of isolated PIC3 chains, spin coated on mica from an organic solution. Scale bar presents the height. Right: AFM-image of a "monolayer" of PIC3 bundles on mica. Scale bars: 250 nm. Taken from Kouwer et al.[25]

(C) Cryo-SEM image of a PIC3 hydrogel. Scale bar: 500 nm. Adapted from Ma et al.[39]

(D) Confocal fluorescence images of PIC3 hydrogels at concentrations of 1 and 0.25 mg/mL. The polymer length is 129 nm for both samples. Scale bars: 5 µm. Reprinted from Vandaele et al.[38]

(E) Confocal fluorescence images of PIC3 hydrogels at 0.5 g/mL. Polymer lengths of 229 nm (long) and 145 nm (short) were used. Scale bars: 5 µm. Reprinted from Vandaele et al.[38]

PIC-BASED HYDROGELS

The gelation of OEG-functionalized PICs is directly related to the properties of the OEG side chains. Hydrophobic interactions between adjacent OEG side chains increase with increasing temperature. Above the LCST, the polymers bundle to give a stable network (Figure 4A).[28] As such, the LCST coincides with the sol-gel transition temperature (or the gelation temperature). PIC polymers formed with 3OEG or 4OEG side chains showed a gelation temperature of ~20°C–25°C (PIC3) and ~42°C–50°C (PIC4),[23] depending on the exact polymer concentration and molecular weight. The increased PIC4 gelation temperature originates from the fact that the longer OEG side chains interact with more water molecules; for longer OEG side chains more energy is thus required to dehydrate the polymer.[29] The gelation temperature around the room temperature make the PIC3 gels very interesting to use. Therefore, most of the research using PIC hydrogels uses PIC3, while PIC4 is used for its macromolecular properties and not so much as a gel.

As it is based on noncovalent hydrophobic interactions, the sol-gel phase transition is reversible. Cooling below the LCST returns the gel to a single-phase solution. The phase separation temperature can be easily tuned by the Hofmeister effect.[30] Results showed that the gelation temperature of a PIC3 hydrogel increased upon adding chaotropic anions, such as ClO_4^-.[31] In contrast, kosmotropic anions, such as Cl^-, were found to decrease the gelation temperature. Using small-angle neutron scattering to characterize the PIC3 hydrogel in different buffers, it was confirmed that ions present in cell culture media also have a direct impact on the assembly of PIC3 hydrogels.[32]

Hydrogel structure

A number of different characterization techniques have been used to unravel the architecture of PIC-based hydrogels.[25] AFM and cryogenic scanning electron microscopy (cryo-SEM) revealed a bundled and fibrous structure of the hydrogel (Figures 4B and 4C).[28] The height measured for each bundle in AFM images showed that an average of approximately seven individual polymers form one bundle. This number is independent of the polymer concentration. This phenomenon is thought to be the result of both the intrinsic chiral nature of PICs as well as the intrinsic stiffness of the polymer.[33] Since the bundle diameter remains unaltered, a higher polymer concentration results in more bundles rather than thicker bundles. More insight into the bundle formation of PIC3 was obtained with small-angle X-ray scattering (SAXS).[34] SAXS was used to study the formation of PIC3 bundles and the link with polymer persistence length. The long polymer fibers that are formed due to the bundling of individual polymers cannot be found in other synthetic hydrogels based on semi-flexible polymers. As a direct consequence of the fibrous structure, the amount of polymer needed to form a hydrogel is very low, i.e., 0.006 wt %. This is 500 times lower than the concentration used for most synthetic hydrogels.[35] It is the fibrous architecture in combination with the high persistence length of the polymers that distinguishes PIC gels from other synthetic hydrogels. From this architecture, the unique biomimetic mechanical properties originate, *vide infra*.

The formation of bundles is a typical structural feature and one of the key properties of biological hydrogels.[36] An in-depth investigation into the structural properties of PIC polymers, such as the influence of hydrophobic interactions, the helical content, and hydrogen bonds was performed.[27] Three alanines were incorporated into each monomer instead of two to yield polyisocyanotripeptides (triPIC) (Figure 3D). These polymers have a very hydrophobic core around the backbone and an increased number of hydrogen bonds between the amide groups of the side chains. The typical bundle formation was confirmed by cryo-SEM and SAXS measurements. Using CD and FTIR spectroscopy, the authors showed that the triPIC polymers are more tightly packed when heated, forming a stiffer hydrogel at 50°C. Another study used triPIC hydrogels to investigate the molecular structure and water dynamics during the gelation process.[37] The findings showed that water molecules are present in between the side chains below and above the gelation temperature. However, during gelation, some water molecules are expelled. The increase in hydrophobic interactions in between the OEG side chains leads to the formation of PIC bundles. Interestingly, once the hydrogel was formed, a small percentage of water molecules remained bound to the OEG side chains due to H bonds. Water can donate two hydrogens to two oxygen atoms of OEG, acting like glue in between the polymers in the hydrogel network.[37]

Despite the key insights obtained, most characterization techniques fall short of visualizing and quantifying the 3D structure of PIC hydrogels *in situ*. AFM, SAXS, SEM, and similar techniques offer very high spatial accuracy (see Box 1). Yet, they provide

Box 1. Characterization techniques for hydrogels

Rheology is the science of deformation and flow. Rheometers are designed to study the response of materials to deformation (liquids, solids, and everything in between, such as gels).[40] When applying a defined amount of stress on the sample, the material response can be readily measured, allowing the calculation of several characteristic parameters. These include elasticity, viscosity, viscoelasticity, poroelasticity, and plasticity. More information regarding rheology is provided in Box 2.

Atomic force microscopy (AFM) is a scanning probe microscopy technique that allows to image and manipulate matter down to the atomic scale.[41] With a sharp cantilever, a surface is probed, the topography is mapped, and a single polymer or molecule can be visualized and/or stretched.[42] The technique is commonly used for structural characterization of biological samples, yielding images with very high spatial resolution. Being a surface technique, 3D information cannot be obtained for thicker hydrogel samples. Additional drawbacks include the lack of universal criteria for probe selection and the potential influence of cantilever characteristics on the results.[43,44]

Small-angle X-ray scattering (SAXS) is a popular technique that allows to characterize macromolecular structures on a very small scale in native conditions.[45] The sample is irradiated with X-rays from one side and the X-rays are collected at the other side by a detector. Electron density distributions cause X-ray scattering. Acquired spectra are often fitted to theoretical models. SAXS typically delivers structural information with a resolution between 0.5 and 100 nm.

Scanning electron microscopy (SEM) is a technique where a focused beam of high-energy electrons is directed to scan a sample under vacuum conditions. The interactions between the electrons and the sample generate secondary electrons, backscattered electrons, and other signals that are detected and converted into a digital image. Using SEM, a resolution down to 1 nm and below can be obtained.[46]

Cryogenic scanning electron microscopy (cryo-SEM) enhances the capabilities of conventional SEM by preserving the native hydrated state of the sample through rapid freezing at cryogenic temperatures. This technique allows for imaging under cryogenic conditions in an electron microscope, thus maintaining the sample's structural integrity to a degree that room temperature SEM may not permit.[47] The imaging technique is similar to SEM and can reach sub-nanometer resolution.[48] However, there are debates whether the original porous structure can be maintained after sample processing.[49]

Fluorescence microscopy is an optical technique to acquire structural or functional images. Upon excitation, the fluorophores present in the sample emit light, with a wavelength longer than that of the excitation source.[50]Using specific optical filters, the excitation light can be blocked from reaching the detector, making it possible to record the fluorescence signal at a very low concentration (down to single molecules).[51] While the spatial resolution of conventional fluorescence microscopy methods is limited by the diffraction of light to 200–300 nm,[52] super-resolution methods, such as single-molecule localization microscopy, can overcome this barrier achieving nanometer-scale resolution.[53]

2D information, or a projection of a 3D environment. This excludes the possibility of measuring dynamical processes *in situ*. By fluorescently labeling the PIC3 polymers, it was possible to use fluorescence microscopy to investigate the 3D structure of PIC-based hydrogels.[38] Making use of available azide moieties, dye molecules carrying dibenzocyclooctyne (DBCO) were coupled in an SPAAC reaction. Confocal microscopy was used to visualize the PIC3 hydrogel network, and the images obtained revealed a very heterogeneous porous structure, similar to biological fibrous hydrogels such as collagen or fibrin (Figure 4). The direct visualization of the network offered the ability to study the impact of experimental parameters, such as polymer concentration and polymer length, on the PIC3 hydrogel network (Figures 4D and 4E). It was shown that polymer concentration has a direct impact on the network architecture at the micrometer scale, while no significant changes were observed when using PIC3 molecules with different polymer lengths.

Box 2. Mechanical characterization of materials

Rheology: rheology is the science of how materials deform when shear forces are applied. Rheometers are used to study the viscoelastic properties of materials. The sample to be measured is confined in a narrow gap between a stationary and a moving part of a measuring cell. In general, two key rheological concepts are used: *stress* (σ) and *strain* (γ). Oscillatory measurements are often used to study the time-dependent properties of viscoelastic materials (Box Figure 2a). For example, by applying small amplitude oscillatory strains or stresses of defined and different frequencies, the *storage modulus* (G') and *loss modulus* (G'') can be determined in different time windows (Box Figure 2b).[40,69] In addition to oscillatory rheology, creep and stress relaxation measurements are used to determine the relaxation time of materials as well as plasticity.

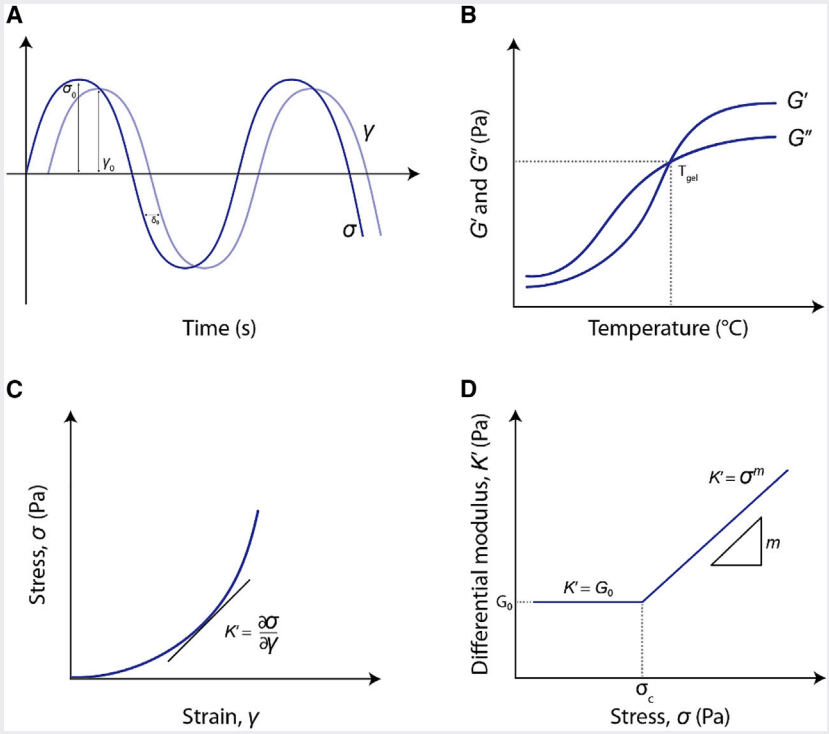

Box Figure 2. Rheology knowhow

(A) Oscillatory protocol for the characterization of viscoelastic materials. The stress and strain follow a sinusoidal function over time. Typically, the shear strain γ is preset and the resulting shear stress σ is recorded. In viscoelastic materials, the two curves experience a phase shift δ.

(B) Characterization of a typical gelation process.

(C) Strain-stiffening behavior.

(D) Transition between the linear and nonlinear regime, observed in a typical pre-stress protocol.

Stress (σ): stress is defined as force per area ($\sigma = F/A$) and has the SI unit of Pa (N/m^2). When the force is applied perpendicular to the axis of the sample so that different layers are sheared past each other, the term shear stress is used.

Strain (γ): strain is defined as the relative deformation, which is the deformation divided by the height or length of the sample system. It is a dimensionless quantity (length/length). Shear strain indicates the extent of deformation after the application of shear stress. We define the shear strain $\gamma = \Delta x/h$, where Δx is the deformation and h the height of the system.

Oscillatory stress: stress can also be applied with oscillatory deformation with frequency ω. When stress and strain are plotted against time t (Box Figure 2a), we can define the amplitude of stress (σ_0) and strain (γ_0) in the function: $\sigma(t) = \gamma_0 (G' \sin(\omega t) + G'' \cos(\omega t))$. In viscoelastic materials, stress and strain are phase shifted by a phase angle δ (Box Figure 2a).

Storage modulus (G'): the storage modulus is a measure of the elastic energy stored in the material during a shear strain cycle. It is directly related to the stiffness of a material. For shear rheology under

sinusoidal conditions, $G' = (\sigma_0/\gamma_0) \cdot cos(\delta)$ (Box Figure 2b). G' can be replaced by the plateau modulus G_0 in a range where G' is independent of the oscillation frequency ω. In elastic materials, G' dominates G''.

Loss modulus (G''): the loss modulus is a measure of the energy lost in a material during a strain cycle measurement because of viscous dissipation in the sample. Under sinusoidal conditions, $G' = (\sigma_0/\gamma_0) \cdot sin(\delta)$ (Box Figure 2b).

Gelation temperature (T_{gel}): the temperature where the value of G' crosses G'' is defined as the precise gelation point of a hydrogel with LCST behavior (Box Figure 2b).

Strain stiffening: strain stiffening describes the nonlinear stiffening response of a material in response to stress or deformation. In a strain-stiffening material, its stiffness is not constant but increases with increasing stress (or strain) after a *critical stress* σ_c is reached (Box Figure 2c). Note that strain stiffening is also known as stress stiffening or nonlinear mechanics.

Differential modulus (K'): the differential shear modulus $K' = \partial\sigma/\partial\gamma$ is calculated from the shear stress σ to the strain γ (Box Figure 2c). In the linear regime, $K' = G_0$; in the nonlinear regime, K' exponentially increases with increasing stress $K' = \sigma^m$, where m is the stiffening index (Box Figure 2d).

Critical stress (σ_c): the critical stress is the stress onset for nonlinearity and determines the sensitivity of the material. A low σ_c implies a high mechanical sensitivity (Box Figure 2d).

Stiffening index (m): in the nonlinear regime $K' = \sigma^m$, the exponent m is referred to as the stiffening index. This index describes the extent of the stiffening response. A high stiffening index causes a rapid increase in stiffness when strain or stress is applied (Box Figure 2d).

Pre-stress protocol: different from a strain ramp protocol, the applied stress is the control variable in the pre-stress protocol. A steady pre-stress σ_0 is applied, onto which a small amplitude *oscillatory stress* is superimposed. The oscillatory stress amplitude used is at most 10% of the steady pre-stress. The pre-stress protocol is sensitive to relaxation. Thus, for materials that exhibit creep, a strain ramp protocol is preferred.[70]

Strain ramp protocol: strain is applied and increased in value linearly in time while the stress response is measured.[70]

Strain softening: strain softening (or strain relaxation) is a material property where a material becomes softer under increased stress (or strain). In fact, it is the opposite effect of strain stiffening.

Stress relaxation: stress relaxation is the response of a viscoelastic material to an applied step strain, where the material undergoes a gradual decrease in stress over time as it relaxes toward its new equilibrium state. During this process, some of the initially stored strain energy is released or dissipated as heat, while the material gradually regains its original mechanical properties.

Plasticity: plasticity is defined as a material's ability to irreversibly deform in response to applied stress.[71] It is quantified by applying stress and observing the point at which the material no longer returns to its original shape after the stress is removed.

Poroelasticity: when a deformation induces a change in the volume of poroelastic materials, they exhibit a time-dependent mechanical response due to water flow into or out of a porous network.[61] Poroelasticity of biological materials is often measured by compression rheology, which measures how these materials deform under compressive forces.

Linear and nonlinear mechanical properties

In addition to mimicking the fibrous structure of biological hydrogels, PIC-based hydrogels also present similar mechanical properties, with a strong nonlinear stiffening response at low stresses[25] (the terminology linked to the characterization of mechanical properties is summarized in Box 2). While still rare, strain-stiffening properties are increasingly observed in soft hydrogels.[54–57] A comprehensive review was recently written by the Gao group.[58] For PIC gels, strain stiffening originates from the semi-flexible architecture of the network, which is a direct result from the high persistence length of the polymers and their (temperature-induced) lateral aggregation. These phenomena have been well described by theory and simulations.[59,60]

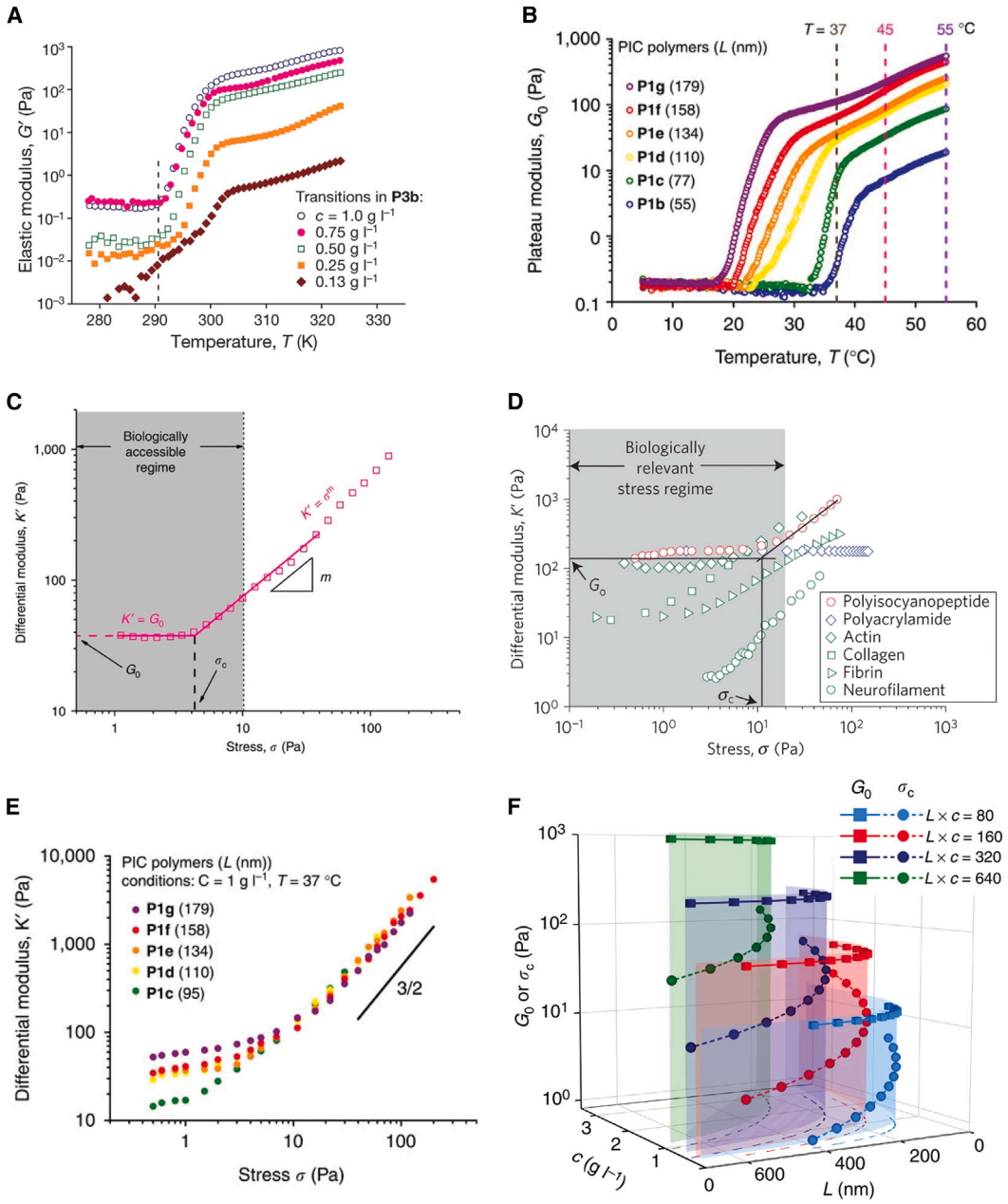

Figure 5. Linear and nonlinear mechanical properties of PIC hydrogels

(A) Plot of the storage modulus G' as a function of temperature for PIC3 hydrogels using different polymer concentrations. The dashed line at T = 18°C shows that the onset of the gelation temperature is nearly concentration independent. Adapted from Kouwer et al.[25]

(B) Plateau modulus G_0 as a function of temperature for PIC3 hydrogels, containing polymers of different length. Reprinted from Jaspers et al.[24]

(C) Stiffness represented by the differential modulus K' as a function of stress σ (PIC3). At low stress, $K' = G_0$. Beyond a critical stress σ_c, K' increases, following $K' \sim \sigma^m$ where the exponent m is the stiffening index. Adapted from Jaspers et al.[24]

(D) Differential modulus K' as a function of stress σ for intracellular and extracellular filamentous biopolymer gels that show strain stiffening. For comparison, the rheology data for a representative synthetic gel (polyacrylamide) and the biomimetic strain-stiffening PIC hydrogel are included. G_0 indicates the equilibrium bulk stiffness and σ_c denotes the critical stress for the onset of strain stiffening of the polymer gel. Reprinted from Das et al.[63]

(E) Plot of differential modulus K' against stress σ for different PIC3 hydrogels consisting of polymers with different molecular weights or polymer lengths L at 37°C. The solid line shows the high stress limit with $m = 3/2$. Reprinted from Jaspers et al.[24]

(F) Interpolated mechanical properties of PIC3 hydrogels are displayed where in a series of gels the product $L \times c$ and G_0 remain constant, but σ_c changes. Four series of hydrogels with constant G_0 are shown in the range of 10–1,000 Pa (squares) and σ_c varies in each series (circles). The projection of the curves on the x-y plane (dashed lines) shows the corresponding lengths and concentrations. Adapted from Jaspers et al.[24]

Rheology tests showed that, for the linear regime, the storage moduli G' of PIC3 hydrogels at the physiological temperature match the stiffness of soft tissues and biological matrices prepared from collagen, fibrin, or Matrigel, ranging from a few up to thousands of pascals. As for any other network made of semi-flexible polymers, the properties of PIC hydrogels depend on polymer concentration c and contour length (of the bundles) L_C. Since PIC gels are thermo-responsive, their stiffness also depends on temperature. As shown in Figures 5A and 5B, the plateau modulus G_0 of PIC3 hydrogels exponentially increases with temperature, concentration, and polymer length. The gelation temperature (T_{gel}) decreases with increasing polymer length, but is independent of the polymer concentration.[24,25]

It is now widely accepted that the mechanical properties of the microenvironment play a crucial role in cellular behavior, and, as such, they are a crucial parameter for cell culture matrices. While most of the scientific literature is still focused on the effect of the material's stiffness, we have to acknowledge the key importance of viscoelasticity and also poroelasticity and plasticity.[61] In addition, it is well known that biological materials constituting soft tissues display nonlinear stiffening responses under (shear) strain.[62] Increasing evidence shows that strain stiffening, the effect where a gel becomes reversibly stiffer under an applied (shear) strain, contributes to cell fate and should be considered as an additional factor. This effect is often overlooked because strain stiffening is relatively difficult to manipulate in biological gels and is rarely found in synthetic gels. PIC-based hydrogels do exhibit strain-stiffening properties and provide different strategies to modify these characteristics.

Strain stiffening can be measured with rheology, using a strain sweep protocol, or preferably with a differential pre-stress protocol (Box 2). This yields the differential modulus $K' = \partial\sigma/\partial\gamma$, where $\partial\sigma$ and $\partial\gamma$ are the superposed oscillatory stress and strain, respectively. For PIC gels and other strain-stiffening materials, the differential modulus K' is constant and equal to the plateau shear modulus G_0 ($K' = G_0$) in the low-stress linear regime while it exponentially increases with stress in the high-stress regime ($K' = \sigma^m$, Figure 5C). The stress at the onset of nonlinearity is defined as the critical stress σ_c (not to be confused with the stress at break, also frequently and confusingly referred to as σ_c). The critical stress is indicative of the sensitivity of the material toward applied stress. The intensity of the nonlinear stress response is described by the stiffening index m. A theoretical upper limit of $m = 3/2$[64] is confirmed by computational simulations.

Experimental data show that PIC hydrogels present a strain-stiffening response in the biologically relevant stress regime where the molecular forces acting in the hydrogel match the forces that cells can apply to their matrix.[65] The properties of PIC hydrogels are also highly similar to gels made of the key extracellular matrix proteins collagen and fibrin (Figure 5D).[66] Importantly, both stiffness G_0 and critical stress σ_c increase with increasing polymer length L_C, following Equations 1 and 2:

$$G_0 \propto {L_C}^2 \quad \text{(Equation 1)}$$

and

$$\sigma_c \propto L_C \quad \text{(Equation 2)}$$

The observed dependencies are perfectly in line with the theoretical predictions for semi-flexible polymers (Figure 5E).[64] The tunability of PIC gels allows to independently manipulate the linear stiffness and the nonlinear strain-stiffening behavior of a sample, e.g., when keeping $L_C \times c$ constant, G_0 remains constant but the mechanical sensitivity to stress σ_c varies with L_C (Figure 5F).[24] In short, both linear

and nonlinear mechanical properties of PIC hydrogels can be readily tuned when altering either the polymer concentration or length.

It should be noted that tissues are subjected to deformations in multiple directions *in vivo*,[67] which are complex and difficult to study *in vitro*. As a result, the number of experimental reports on strain stiffening is limited and mostly accompanied by computer simulations. The mechanical response was studied when multiaxial deformation was applied to PIC3 gels.[68] It was shown that the polymer concentration did not affect axial strain-induced softening/stiffening behavior. However, the persistence length of the polymer was found to influence the compression softening behavior of PIC3 gels.

TUNING HYDROGEL PROPERTIES

Given the synthetic nature of PIC hydrogels, their mechanical and structural properties are readily adjusted to meet the requirements of specific applications. In this section, we provide an overview of two principally different approaches to obtain hydrogels with different properties.

Chemical and physical crosslinkers

The mechanical properties of PIC-based hydrogels are easily modified by introducing chemical or physical crosslinkers into the network. The influence of dimensions of chemical crosslinkers on the structure, mechanics, and gelation temperature of PIC3-based hydrogels was investigated.[72] In this work, PIC3 polymers decorated with azide moieties were mixed with different homobifunctional DBCO crosslinkers below T_{gel}. The SPAAC-based crosslinking reaction occurred within a couple of minutes, yielding stable hydrogels that lost their thermo-responsive nature (Figures 6A and 6B). SAXS measurements showed that, in the recooled crosslinked PIC3 gel, only the thickest bundles remained, while rheology experiments showed that the linear and nonlinear mechanical properties barely changed at lower temperatures. The authors concluded that the mechanical load is predominantly carried by the thickest fiber bundles, while thinner bundles have almost no contribution to the mechanical properties of the hydrogel network.

In this case, crosslinking between the polymer chains inside a bundle may not fully prevent network dissolution upon cooling, and the crosslinks do not significantly contribute to the mechanical properties since the network architecture remains unchanged. Larger crosslinkers, for instance, iron oxide nanoparticle-based crosslinkers are also able to crosslink between polymer bundles. Inter-bundle crosslinking does affect the mechanical properties significantly and the shear modulus of a PIC3 gel can be increased significantly. DBCO-functionalized rod-shaped nanoparticles were used as a crosslinker in the hydrogel.[73,74] It was shown that the plateau modulus, G_0, increased after crosslinking the network and that stiffer hydrogels displayed a higher threshold to enter the stiffening regime. SEM experiments suggest the formation of a highly porous polymer-particle network composed of much thicker bundles. As a result, the stiffness can increase up to 40 times (reaching into the kPa regime), while the polymer/nanoparticle concentration is kept to a minimum (both 0.1 wt %).

While chemical crosslinkers can be used to tune the mechanical properties of the hydrogel, their irreversibility may present a drawback. Using the same rod-shaped nanoparticles to obtain physical crosslinking, the same degree of stiffening was not observed as was found for the covalently crosslinked materials; however, the

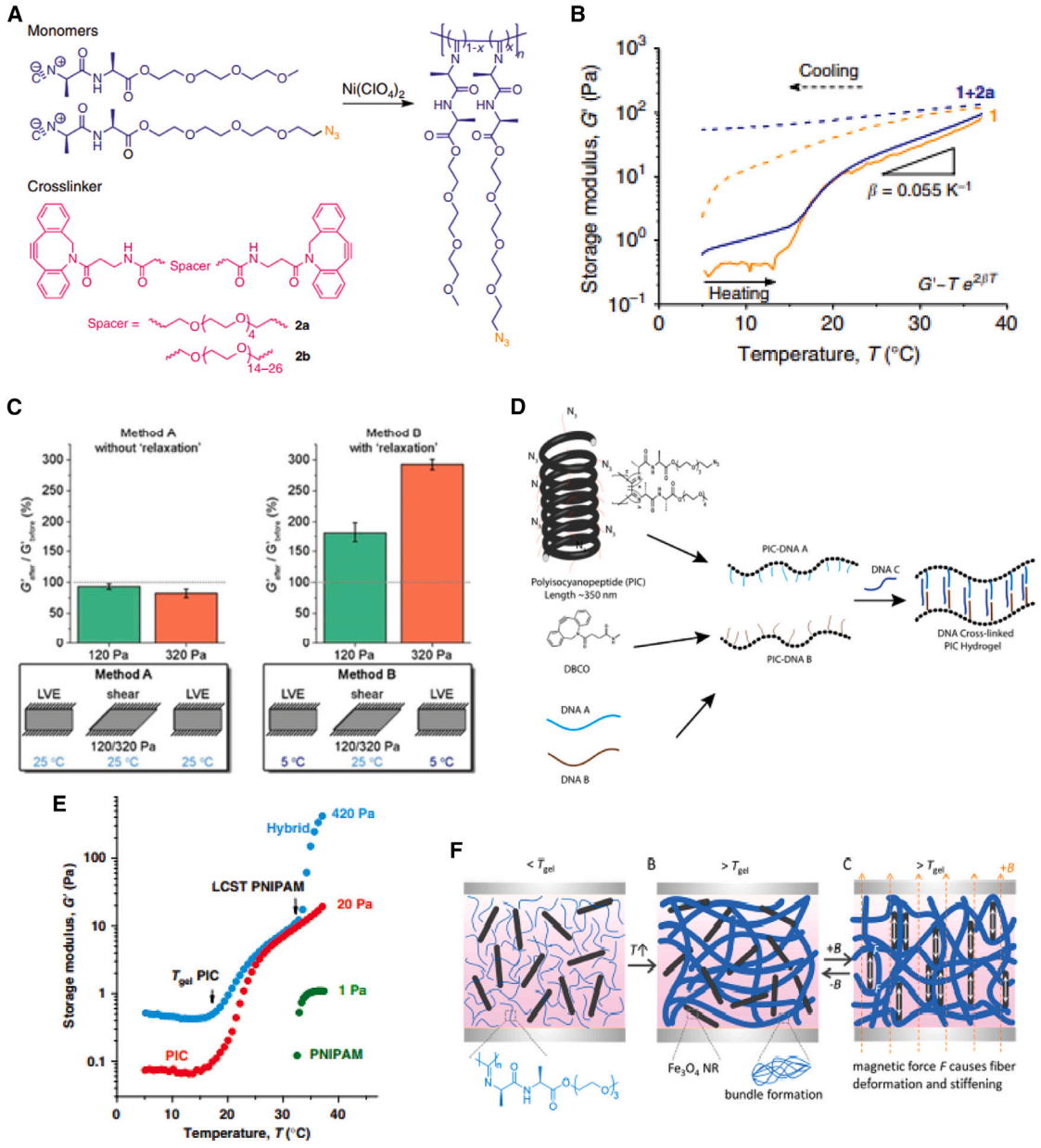

Figure 6. Examples of tunability of PIC

(A) Monomers with and without azide function were used to synthesize the PIC (blue). In magenta two DBCO-spacer-DBCO crosslinkers are shown with one short spacer and one long space. Adapted from Schoenmakers et al.[72]

(B) The mechanical properties of intra-bundle crosslinked PIC hydrogel (blue) are compared with the mechanical properties of a non-crosslinked hydrogel network (orange). The solid lines represent heating and the dashed lines cooling down of the samples, showing that the crosslinked hydrogel remains a gel after cooling down. Adapted from Schoenmakers et al.[72]

(C) The recovery of G′ after applying stress below (120 Pa) and above (320 Pa) the plateau modulus for DBCO-functionalized CCMV capsid crosslinkers at 25°C (left) and 5°C after allowing re-crosslinking (right). Reprinted from Schoenmakers et al.[75]

(D) The preparation protocol for DNA-responsive PIC hydrogels is displayed. Azide-functionalized PIC polymer is conjugated to ssDNA-DBCO, whereafter different types of complementary crosslinker DNA strands are used to form a hydrogel. Adapted from Deshpande et al.[76]

(E) The thermo-responsive mechanical properties are shown of PIC, pNIPAM, and the PIC-pNIPAM hybrid hydrogel. Adapted from de Almeida et al.[77]

(F) PIC is mixed with magnetic nanorods and allowed to form a hydrogel. Applying a magnetic field allows particles to align and induce fiber deformation. Adapted from Chen et al.[78]

hydrogel displayed self-healing properties.[74] Crosslinkers based on virus-like nanoparticles were also applied to PIC.[75] The empty protein shell from the cowpea chlorotic mottle virus was equipped with DBCO groups and subsequently used to crosslink the hydrogel. While the bond between one capsid protein and the PIC polymer is covalent, the virus particles themselves can (dis)assemble. When stress was applied to the hydrogel, the capsids were (partially) pulled apart and smaller subunits were formed. Since some capsid proteins contained unreacted DBCO groups, new crosslinks could form (provided that these protein building blocks have enough mobility). Cooling down the hydrogel after a period of stress allowed these free DBCO groups to react with unoccupied azide moieties, resulting in the local "healing" of damaged areas. When comparing the modulus of the cooled hydrogel before and after deformation, a 3-fold increase of the modulus was observed (Figure 6C).

While the virus capsids form crosslinks with unknown stoichiometry, more recent efforts have introduced specific physical crosslinks with a clearly defined 1:1 stoichiometry. For instance, a highly specific heterodimeric coiled coil with known thermodynamic and kinetic properties was used. Each coiled-coil-forming peptide was functionalized with DBCO at one terminus so that the folded coiled-coil dimer carried exactly two DBCO functional groups.[75]

Along this line, a similar strategy was applied to investigate the effect of a physical crosslink on the mechanical properties of PIC4 hydrogels. Highly defined hydrogel networks based on four-arm poly(ethylene glycol) (starPEG) were chosen as control.[79] The relaxation time of the coiled-coil-crosslinked PIC network, which maintained its strain-stiffening properties, was two orders of magnitude longer than that of the corresponding starPEG network. This indicates that the crosslink properties in combination with the network topology determine the stress relaxation behavior of the network. Specifically, interactions within bundling slow down the relaxation of network chains, suggesting that local dynamics are coupled to the overall network structure.

Similar to coiled coils, DNA oligonucleotides form highly specific crosslinks and provide access to the entire toolbox of DNA nanotechnology. For instance, PIC4 polymers were functionalized with single-stranded DNA and introduced complementary DNA strands with different lengths (22–32 nucleotides) as crosslinkers.[80] No hydrogel formation was observed when the DNA strands were not complementary. When applied to short PIC4 polymers (133 nm) only weak hydrogels were formed (T_{gel} > 50°C), while long polymers (335 nm) formed hydrogels at 39°C. Furthermore, pH-sensitive DNA crosslinkers and a DNA aptamer that binds to human α-thrombin were also applied to yield hydrogels mechanically responsive to their environment. Following an analogous DNA-based crosslinking strategy, DNA-crosslinked hydrogels were also formed using different PIC polymers decorated with complementary ssDNA strands[76] (Figure 6D). The extent of base pair overlap directly determines the linear and nonlinear mechanical properties.

Hybrid networks

A commonly used approach to tune hydrogel properties is to make a composite material where the second component can be another polymer, fibers, or solid particles. The Koenderink lab showed how the architecture of the PIC hydrogel can be tuned when adding fibrin.[81] Their PIC3/fibrin hybrid displayed a more heterogeneous structure with thicker fibrin fibers when compared with the pure fibrin sample. Moreover, both components contributed similarly to the stiffening response, which was roughly the weighted sum of the individual components. A higher fibrin content reduced the stress response, as the stiffening index of fibrin gel is much lower than

that of PIC3 hydrogels. In a more systematic study, Jaspers et al. compared composites made from PIC3/fibrin, PIC3/polyacrylamide (PAA), and PIC3/carbon nanotubes (CNTs).[82] These components are semi-flexible, flexible, and stiff, respectively, dramatically impacting the properties of the materials obtained. Introducing stiff CNTs resulted in a much stiffer hydrogel that was also more sensitive to stress. In contrast, introducing a flexible polymer, PAA, increased the hydrogel stiffness in the linear regime but decreased the stiffness in the nonlinear regime. While PAA offered greater flexibility for modifications, including adjustments in polymer concentration and crosslinking density, it concurrently impacted the architecture of the PIC hydrogel by reducing its porosity.

It was further observed that the linear storage modulus (before deformation) was merely a linear combination of the two components when no interaction between the two gels was present, while the nonlinear behavior was an intermediate state influenced by both components. When deformation was applied to the system, both networks deformed independently while also contributing to the nonlinear stiffening response of the hybrid hydrogel. When interaction occurred between the two systems, e.g., in the form of chemical crosslinkers, one of the two components dominated the overall response.

The PIC gel is stress stiffening. When the second component in the hybrid network is a responsive material that induces deformation, one may expect an extremely strong mechanical response of the composite gel. An ultra-responsive hybrid hydrogel was prepared by combining the strain-stiffening PIC3 network with the thermo-responsive flexible network of poly(*N*-isopropylacrylamide) (pNIPAM).[77] Upon heating the (semi)interpenetrating network beyond the LCST of pNIPAM, pNIPAM collapses and creates internal stress that causes the PIC network to stiffen. As a result, the storage modulus of the composite increases up to 50 times compared with the original modulus within a few degrees (Figure 6E). The authors estimated an average of around 1 pN of force applied per average network fiber; a value that is similar to forces applied in biological tissues. The stress applied in the polymer hybrid system scales linearly with the concentrations of both PIC3 and pNIPAM. Since the collapse of pNIPAM is triggered by an increase in temperature, using a PIC/pNIPAM hybrid network allows scientists to gain precise control of the mechanical properties of the hybrid hydrogel, making it an ideal scaffold for biological applications that require dynamic control of material stiffness.

Temperature, however, is not an ideal cue in biology and Chen et al. used the same approach but with a magnetic stimulus. They prepared a hybrid of PIC3 with submicron-sized magnetic iron oxide nanoparticles. Upon exposure to a (small) external magnetic field, the particles aligned and strained the PIC network, resulting in a dramatic increase of the stiffness of the composite (Figure 6F),[78] analogous to the pNIPAM hybrids. Note that for both responsive composites, temperature- or magnetic field-induced stiffening is reversible: as soon as the cue is removed, the modulus drops again. Apart from stiffening, the iron nanorods also gave rise to a conductive and magnetic hydrogel, opening doors toward more responsive and controllable materials. A more in-depth study showed that the anisotropy of the nanoparticles is transduced toward the polymer network once a magnetic field is applied.[83]

For biological experiments, PICs have been mixed with Matrigel (Box 3). As there is not a strong interaction between the two materials in these composites, no major effects on the mechanical properties were observed and G' is merely the sum of the

Box 3. The gold standard: Matrigel and equivalent basement membrane extracts

A wide range of scaffolds for cell culture are commercially available worldwide. Matrigel is one of the best-known and most widely used hydrogel materials for biological applications involving cell culture, tissue engineering, organoid growth, and therapeutic screening.[122] This hydrogel is an extract of the basement-membrane matrix from Engelbreth-Holm-Swarm mouse sarcomas and contains several biological polymers, where laminin, collagen IV, entactin, and heparin sulfate proteoglycan perlecan[122,123] are the most prevalent. Besides these biopolymers, Matrigel is composed of a largely unknown mixture of thousands of peptides, proteins, and growth factors, which influence cellular behavior.[124,125] The main advantage of Matrigel is its high activity and biocompatibility, as it presents natural binding motifs for different cell types. In addition, it is very easy to use due to its thermo-responsive characteristics.[126] However, there are also drawbacks associated with the use of Matrigel, among which the major one is that, as an animal-derived material, there is batch-to-batch variability[127] and it is therefore unsuitable for clinical applications due to its tumorigenic nature. Furthermore, the structural and mechanical properties of Matrigel are not comparable with fibrous hydrogels such as collagen or fibrinogen. From a mechanical perspective, Matrigel lacks both strain-stiffening behavior as well as a heterogeneous fibrous environment.[128–130]

two components.[84] In the next sections, we further discuss the biological applications of materials based on PICs only, unless mentioned otherwise.

APPLICATIONS OF PIC POLYMERS AND PIC-BASED MATERIALS

The growing interest in PIC polymers and their hydrogels stems from their unique biomimetic properties, which render them highly appealing for a diverse array of biological applications. Here, we describe several key applications, with a special focus on 3D cell culture.

Cell culture and mechanobiology studies

Hydrogels are an excellent choice for mimicking extracellular matrices. A qualified synthetic biomimetic matrix needs to fulfill three requirements: (1) compatible 3D structure, (2) suited mechanical feedback toward cellular forces, and (3) bioactive handles that allow cells to directly interact with the network.[85] As already described in section "PIC-based hydrogels", PIC hydrogels are characterized by a heterogeneous, noncovalently crosslinked, porous network and simultaneously display linear and nonlinear mechanical properties similar to biological tissues. To use this material as a cellular matrix, one criterion is missing: cell-adhesion motifs. These are easily attached to azide-decorated PIC polymers. Cell-adhesive peptides, such as arginyl-glycylaspartic acid (RGD), hormones,[86] or proteins,[87] can be covalently coupled in an SPAAC reaction when these bioactive molecules are equipped with a cyclooctyne DBCO or BCN (bicyclononyne) functional group.[88] In this light, the PIC3 hydrogel can be seen as a minimalist synthetic biomaterial that can be modified as desired for the development of advanced 2D and 3D cell cultures.

Indeed, PIC3 hydrogels have been used as culture systems for a large number of different primary cells and cell lines[39,89–93]: mesenchymal stem cells (MSCs), fibroblasts, endothelial and epithelial cells, osteoblasts and various immune cells, among others. While PIC3 hydrogels also support 2D experiments, most researchers use it for 3D cultures where they can fully exploit the thermo-responsive properties of the gel to easily extract the cells at the end of an experiment. Cell viabilities are typically very high[63] (> 90%) and cells have been cultured for up to 28 days without significant loss in viability,[92] although the gel may contract at some stage due to cellular contractile forces. For cells with strong cell-matrix interactions, e.g., MSCs[89] and fibroblasts,[94] the gel properties will directly influence cell morphologies and fate, which allows one to control and steer cell behavior as desired. In addition, these cells readily

migrate through the PIC3 networks using physical remodeling mechanisms.[65] In contrast, cancer cells with strong cell-cell interactions are relatively insensitive to the gel properties[89]; they proliferate into multicellular spheroids as long as growth is not blocked by a too stiff matrix.

Besides the development of "straightforward" 3D cell cultures, increasing attention is focused on PIC3 matrices for more complex 3D cell culture models such as organoids and assembloids.[90,91] Preliminary results from cultures of various murine and human healthy and cancerous tissue organoids have indicated that PIC3 hydrogels support expansion. But, for full differentiation, additional biochemical cues may be needed, for instance, laminin and glycosaminoglycans, which are abundantly present in Matrigel.[91] It should be stressed, however, that comparing organoid cultures in PIC and Matrigel matrices may not be too relevant. Matrigel-based cultures often mimic (cells from) the native tissue insufficiently, possibly because of the lack of a fibrous architecture and the related nonlinear mechanical characteristics.

The unique mechanical properties of PIC hydrogels have triggered the extensive use of this material in mechanotransduction studies. Directly interacting with their surroundings, cells sense and respond to the linear and nonlinear mechanical properties of their environment.[66,95] The ECM contributes key parameters to control cellular behavior, namely adhesion, shape, spreading, differentiation, proliferation, and migration.[96] Stiffness has long been thought to be the main regulator of cell behavior; however, more recent insights indicate that also other mechanical properties, such as viscoelasticity and strain stiffening, play a critical role in cellular regulation.[61,97] Making use of the unique tunability of PIC3-based hydrogels, the influence of mechanical and biological cues on morphology,[89] mechanotransduction,[98] paracrine function,[99] and differentaiton[63] of (stem) cells were disentangled systematically. The use of PIC3 hydrogels, based on polymers with different contour lengths,[93] as well as hybrid hydrogels made of PIC/fribin[81] or PIC/Matrigel,[84] provides additional possibilities for obtaining a deeper understanding of mechanobiology (in particular on the biological effects of nonlinear mechanics) and opens up new routes for the co-culture of different cell types.

Cells continuously sense mechanical cues in their microenvironment (neighboring cells and ECM) and, in turn, generate contractile forces, which stiffen and remodel the matrix. The cellular response depends on the amount of mechanical stress and rate of deformation to which the cell is subjected.[95,100] Focal adhesions, which contain integrin receptors, link the ECM to the cytoskeleton and allow direct force transmission between mechanical structures inside and outside the cell.[101] More in-depth studies revealed that cells recruit ECM fibers, thereby pushing, pulling, and remodeling their microenvironment.[102] It has been proven that the properties of the individual fiber architecture play a crucial role in regulating cellular behavior.[81,103] The biomimetic nature of PIC hydrogels enables the systematic investigation of the influence of specific matrix properties on cellular responses. Most recently, Yuan et al. demonstrated that PIC3 hydrogels, as a fully synthetic material, are able to recreate the complicated bi-directional cell-matrix interactions in nearly all aspects, including cellular force-induced fiber remodeling and long-range force propagation.[65] Representative mechanobiological studies using PIC3 hydrogels are summarized in Figure 7.

Coatings

Hydrogels are an interesting material for biomedical coating applications. They can improve the biocompatibility of materials, lubricate surfaces, or introduce (bio)active functionalities for further applications (e.g., drug delivery,

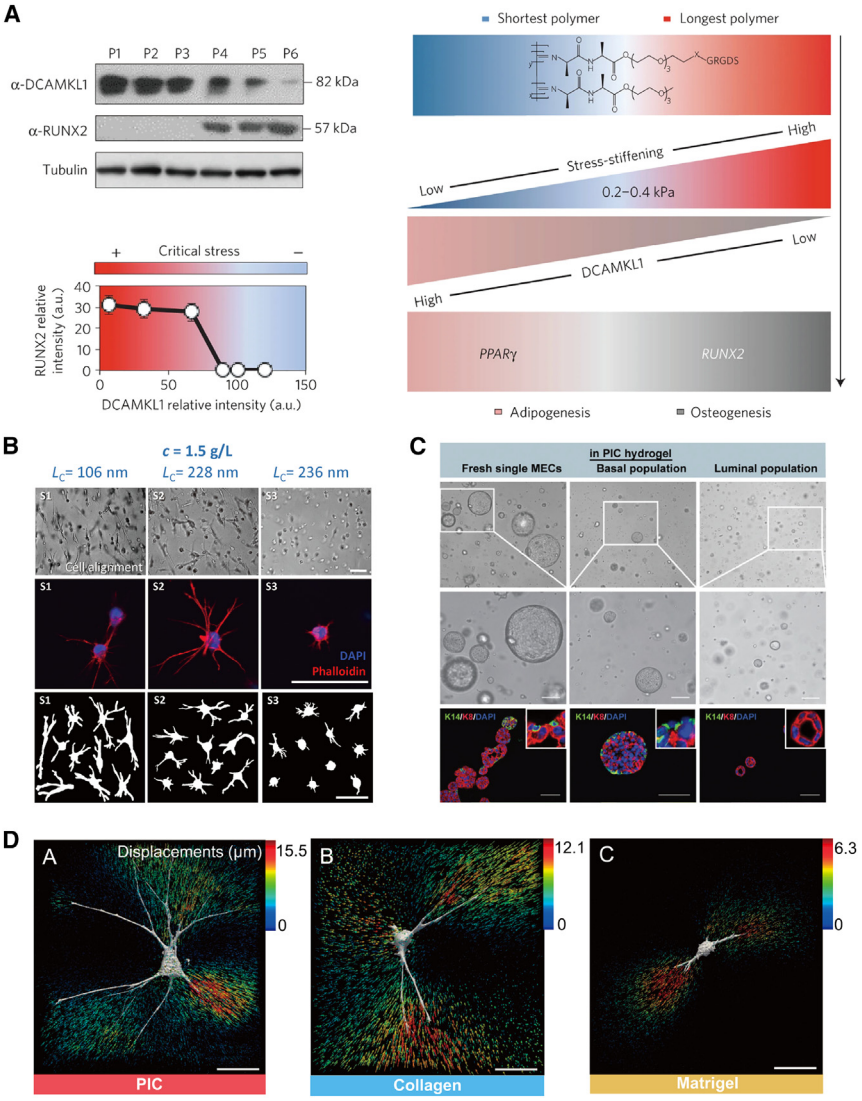

Figure 7. Applications of PIC hydrogels in mechanobiological studies

(A) Microtubule-associated protein DCAMKL1 is involved in stress-stiffening-mediated stem cell differentiation. Adapted from Das et al.[63]

(B) Impact of polymer length (nonlinear mechanics) on the spreading of human adipose-derived stem cells (hASCs). Scale bars: 70 μm. Adapted from Liu et al.[89]

(C) Representative bright-field and immunofluorescence images of mammary gland organoids (MGOs) generated from unsorted mammary epithelial cells (MECs) (left), purified basal cells (middle), and luminal cells (right) in PIC hydrogels. Scale bars: 50 μm. Adapted from Zhang et al.[91]

(D) Comparison of cell behavior and cell-matrix mechanical interactions between PIC and biological matrices. hASC-induced 3D matrix displacement fields in hydrogels made of PICs (A), collagen type I (1.2 mg mL^{-1}) (B), and Matrigel (70%) (C). The color of the arrows indicates the magnitude of the local displacement vector. Scale bars: 50 μm. Adapted from Yuan et al.[65]

biosensing).[104,105] When using hydrogels as coatings, possible drawbacks are their biodegradability and the sometimes-poor adhesion to material surfaces. The adhesion of hydrogels can be easily improved, however, when the polymer of interest is covalently attached to the surface to yield a polymer brush.[105,106] The use of PICs as a coating material has one unique advantage: since the polymer is semi-flexible, it will not collapse when grafted on surfaces. When PIC3 hydrogels were

covalently grafted on surfaces, the hydrogel layer could be functionalized and used as a biosensor to detect and convert biological reactions into signals, allowing precise monitoring of biomolecules, pathogens, and cell metabolites.[107,108]

3D printing

A more recent, newly emerging area toward biological applications of hydrogels is (3D) bioprinting where the material (referred to as bio-ink) is printed to achieve a desirable 3D macroscopic shape.[109] Given the rapidly evolving applications of 3D printing[110] and the search for novel bio-ink formulations, it is interesting to look at the possibility of using PICs. A new technique to 3D print PIC3 polymers was introduced by mixing them with PIC3-gelatin methacrylate hydrogels.[111] Compared with other commercially available bio-inks, such as Pluronic F-127, the concentrations required are up to 40× lower, resulting in a higher cytocompatibility. Their results showed that printing PIC3 hybrid hydrogels presents several benefits, including easy deposition and removal of the gel, and the fabrication of stable hydrogel prints at 37°C. Despite this progress, the key challenge remains to produce a biocompatible, printable bio-ink that possesses all the important properties of a biological hydrogel.[112]

Antibacterial applications

Besides serving as a cell culture platform, PIC3 hydrogels were found to be suitable as an antibacterial scaffold in wound dressing and tissue engineering applications. Given the well-known role of reactive oxygen species (ROS) in triggering cell death, several works have reported hydrogels that can generate ROS with a controllable trigger (e.g., light).[113] By conjugating responsive motifs to the PIC3 backbone, such as cationic oligo(p-phenylene vinylene),[114] oligo-electrolyte,[115] polythiophene,[116] and nanoparticles,[117] promising antibacterial effects were reported.

Drug delivery

Given the high biocompatibility of PIC3 hydrogels, the interest in using this material for clinical applications has grown in the last few years. Here, we provide an overview of some pre-clinical studies published, but more are currently ongoing. A new therapy was proposed for patients requiring periodontal treatment, where doses of medication can be altered and adjusted by incorporating bioactive agents into poly(lactic-co-glycolic acid) microspheres dispersed in PIC-based hydrogels.[118] More recently, Wang et al. optimized the system by introducing antimicrobial and anti-inflammatory components and investigated the effects of this material *in vivo*.[119] The results confirmed that the PIC3 hydrogel can be used as a safe vehicle for drug delivery in the periodontal pocket.

Wound healing

Given their fibrous structure and biomimetic mechanical properties, PIC3-RGD hydrogels have been used to study fibrosis and scar formation.[94] Moving closer to clinical applications, a recent study has shown that PIC3 hydrogels can be used as a platform to restore the function of primary vaginal fibroblasts.[92] The potential of using PIC3 hydrogels in wound healing applications was first shown by the Wagener group.[120] Further research by Op't Veld and coworkers included experiments where wounds were covered with a non-functionalized PIC3 hydrogel, an RGD-functionalized PIC3 hydrogel, and Matrigel as a control.[121] It was found that the PIC-based hydrogels did not induce a strong inflammatory response in the wounds.

Taken together, these results support the potential of using PIC3 hydrogels for wound healing applications. Independent of the specific application, before being administered in patients PIC polymers must meet certain requirements.[131] To that end, Walboomers' lab compared several commonly used sterilization methods

and investigated their effect on the properties of PIC3 hydrogels.[132] The authors concluded that the use of both UV light and supercritical CO_2 had no influence on the structural and mechanical properties, while autoclaving or γ irradiation were found to alter these properties. A fully sterilized hydrogel, suited for clinical studies, was achieved using supercritical CO_2.

IMMUNOLOGICAL APPLICATIONS OF PIC POLYMERS

Artificial antigen-presenting cells

Many biological processes start with the binding of a multivalent ligand to membrane-bound cell receptors. The unique semi-flexibility of water-soluble PICs make them an interesting candidate to mimic the multivalent presentation of biological signals to cells. For this purpose, PIC4 polymers are ideal as they are soluble at a physiological temperature of 37°C. During the interaction of immune cells, such as dendritic cells (DCs) and T cells, multivalency is extremely important.[133,134] DCs are used in the clinic for immunotherapy and, despite enormous success, their widespread application is hampered by a labor-intensive *ex vivo* cell expansion process and associated high costs. Furthermore, the quality of the generated cells depends on the quality of the immune cells taken from the patient. For this reason, artificial scaffolds, so-called artificial antigen-presenting cells (aAPCs), have gained much attention as cheap, off-the-shelf alternatives for DCs.[135–138]

PIC4 has been extensively exploited for aAPC use. To mimic the function of DCs, three signals are important: (1) stimulation of the T cell receptor (TCR), (2) co-stimulation to further activate and differentiate the T cells, and (3) cytokines, which stimulate important processes, such as T cell survival. As a proof-of-concept, anti-CD3 (αCD3) antibodies, which are known to polyclonally trigger the TCR, were bound to PIC4, making use of the streptavidin-biotin interaction or the SPAAC reaction as described above.[84,139] T cells stimulated with αCD3-functionalized PIC4 were activated at lower concentrations and displayed a stronger T cell response compared with soluble αCD3 controls[139] (Figure 8A). Furthermore, these experiments demonstrated that the PIC4-based system is biocompatible and non-toxic *in vitro*. In an effort to understand this new class of aAPCs, the specific influence of polymer length and antibody density on the T cell activation process was investigated. It was found that polymers with a higher antibody density activate T cells at lower concentrations and that polymer length is another crucial parameter.[142]

To better mimic DCs, the PIC4-based aAPC was decorated with αCD3 to trigger the T cell response and anti-CD28 (αCD28) antibodies as a co-stimulus (Figure 8B).[143] The critical threshold concentration of antibodies required to trigger a T cell response was lower and more specific for the semi-flexible PICs co-functionalized with both antibodies than when soluble antibodies were used. This finding indicates that the PIC4-based synthetic aAPC is more efficient when compared with existing aAPCs. Subsequently, the PIC4 polymer was used to compare a total of six different co-stimulatory molecules. This research concluded that CD28 and CD2 are the main players in T cell priming, a process where T cells upregulate activation markers, secrete cytokines, and start to proliferate.[144] More importantly, the way how co-stimulatory signals are presented has a direct impact on signaling pathways involved in priming. This includes both the timing of signal exposure as well as the amount and composition of molecules.[145]

Going one step further, cytokines were attached to PIC4-based aAPCs (signal 3 described above). Cytokine-based anti-cancer therapies have low efficacy and frequently induce toxic side effects due to a systemic and non-specific

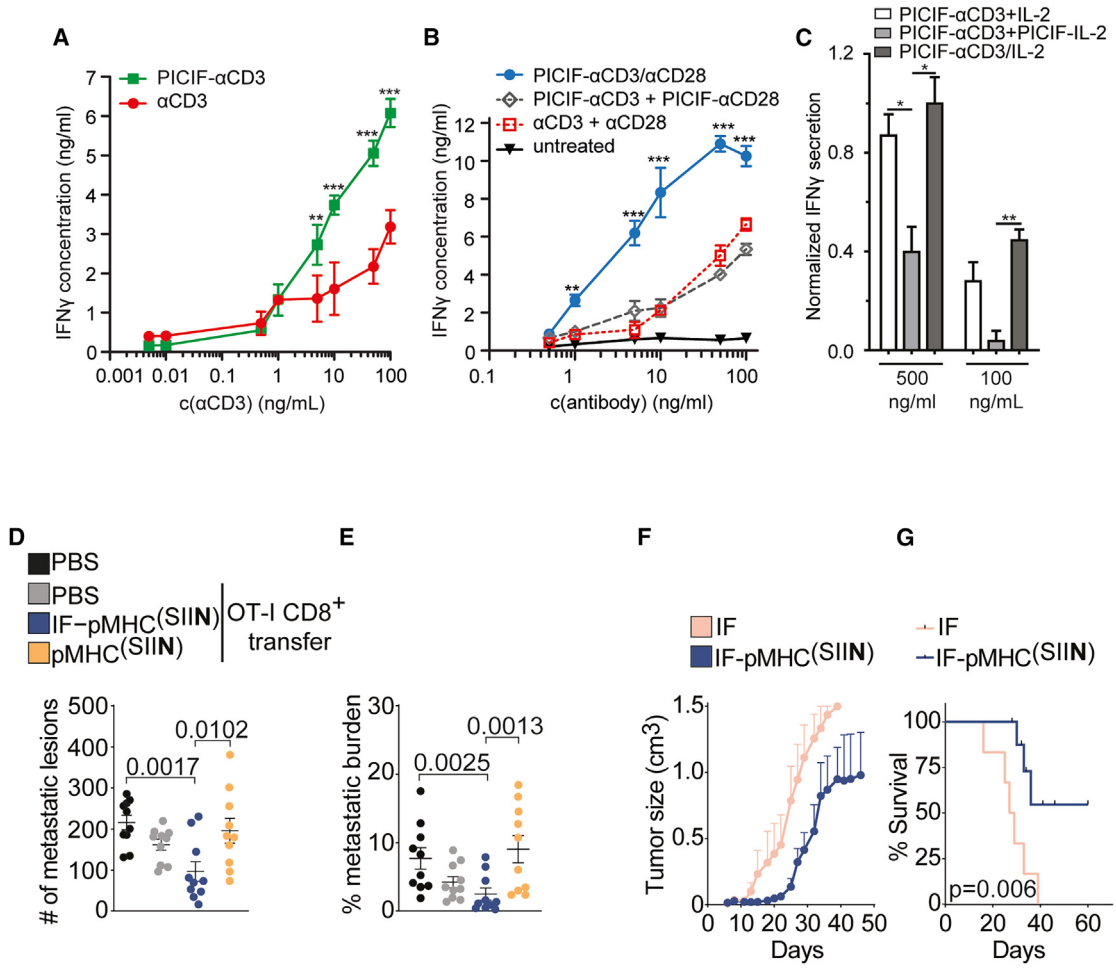

Figure 8. T cell activation and anti-tumor studies

T cell activation and anti-tumor effects of differently functionalized nanosized PIC4 immunofilaments *in vitro* (A–C) and *in vivo* (D–G).

(A) IFN-γ secretion (measurement for T cell activation) by T cells stimulated with soluble αCD3 or αCD3 bound to PIC4 (PICIF-αCD3). **, ***p < 0.01, 0.001. Adapted from Mandal et al.[139]

(B) IFN-γ secretion of T cells treated with soluble αCD3/αCD28 or PIC4 functionalized with both antibodies (PICIF-αCD3/CD28). **, ***p < 0.01, 0.001. Adapted from Mandal et al.[143]

(C) IFN-γ secretion of T cells treated with PIC4 functionalized with αCD3, IL-2, or the combination. *, **p < 0.05, 0.01. Adapted from Eggermont et al.[140]

(D and E) (D) Number of metastatic lesions and (E) metastatic burden in lungs of mice receiving adoptively transferred OT-1 T cells followed by soluble or PIC4 functionalized pMHC treatment. After treatment, B16-OVA tumor cells are injected.

(F and G) (F) B16-OVA tumor size and (G) survival of mice treated with soluble or PIC4 functionalized pMHC. Here the tumor is grown first, followed by treatment. (D–G) Adapted from Weiss et al.[146]

administration. A possible solution to this is to locally concentrate cytokines at the tumor, e.g., using PIC4-based aAPC scaffolds. To this end, PIC4 was functionalized with αCD3 and interleukin-2 and this multifunctional polymer induced stronger T cell activation compared with PIC4 with αCD3 alone (Figure 8C).[140] In addition, the combination of αCD3 and interferon-α induced long-term T cell proliferation. A direct comparison of PIC4-based scaffolds and decorated microbeads clearly showed a stronger response when the PIC4 scaffold was used. This is direct evidence that the semi-flexible nature of the polymer scaffold, which enables multivalent binding, is a crucial property for the development of PIC-based aAPCs.[139–141]

Most recently, the anti-tumor effect of nanosized immunofilaments made of PIC4 polymers has been validated *in vivo*. Using polymers functionalized with peptide

major histocompatibility complexes (pMHCs) for the activation of antigen-specific T cells inhibited the formation of melanoma metastases, which is a milestone toward clinical applications in the future. In addition, in a therapeutic model these pMHC-functionalized PIC4 polymers reduced primary tumor growth (Figures 8D–8G).[146]

Another example was published by Hammink and co-workers where magnetic microbeads were grafted with PIC4 brushes, functionalized with αCD28 and αCD3.[147,148] This system is straightforward to purify due to the magnetic properties of the beads and requires less antibodies to induce a higher degree of activation (compared with solely antibody decorated beads). The fact that this system is more efficient indicates that both the architecture and flexibility of the PIC4 brushes are important for a higher activation, showing the importance of a decent scaffold.

Other applications

Apart from T cell activation, the PIC4 scaffold has been used to target leukemia cells. When decorated with DNA aptamers targeting leukemia cells, PIC4 scaffolds were found to inhibit the growth of the cancer cells with minimal off-target effects.[149] The potential of PIC4 to mimic naturally occurring multivalent interactions was further demonstrated where autoreactive B cells of rheumatoid arthritis (RA) patients were targeted with PIC4 scaffolds.[150] In this case, the PIC4 was decorated with cyclic citrullinated peptides (CCPs), which specifically bind anti-citrullinated protein antibody (ACPA)-expressing B cells, a hallmark for RA. ACPA B cells were selectively bound and stained by the CCP-PIC4 polymers. Furthermore, silencing of the ACPA B cells was achieved by triggering CD22, a B cell-specific inhibitory receptor, with CCP-PIC4 polymers functionalized with a CD22 ligand. Again, this demonstrates the advantage of co-functionalizing multivalent scaffolds.

CONCLUSIONS AND OUTLOOK

Polymers with a helical structure often render a wide variety of unique properties,[11] including PICs. Further modification of PIC polymers with OEG increases their water solubility.

The PIC hydrogels offer key advantages over other biological and synthetic soft materials. In short, their synthetic nature offers full control and high tailor ability of the architecture and mechanical properties of the gel. In addition, similar to other synthetic materials, gel formation is highly reproducible and xeno-free. As opposed to other synthetic hydrogels, though, PIC gels possess the architecture and mechanical properties that are also found in nature. These properties are known to play crucial roles in guiding complex cell-matrix interactions and ultimately regulating cell function, communication, and development.[61,151,152] Moreover, for cell culture applications, the thermoreversible properties of the PIC gels are extremely useful to extract cells and cell constructs, such as organoids, from the matrix without the need to add adverse enzymes or other chemicals; after cooling the cells are simply separated by centrifugation.

PIC3-based hydrogels ideally mimic the properties of natural ECM polymers, including network architecture, linear mechanical properties, and strain stiffening. Undoubtedly, the large body of work on PIC3 properties has shown that this synthetic material is highly biomimetic. It thus serves as an excellent platform to further disentangle the interplay between these physical parameters and biochemical cues. With regard to an *in vivo* use of PIC3 hydrogels, some key technical features, e.g., degradation, are yet to be determined.

Beyond functional hydrogels, soluble PIC polymers have further been harnessed to create artificial antigen-presenting cells. Highly promising results have confirmed the efficacy of PIC4-based immunofilaments in both *in vitro* and *in vivo* settings. Nonetheless, additional research into their *in vivo* efficacy and toxicity profiles is imperative before PIC4-based polymer scaffolds can advance toward clinical applications.

In summary, we anticipate a bright future for PICs as a versatile family of functional polymer materials, well positioned to make substantial contributions to both fundamental research and clinical applications.

ACKNOWLEDGMENTS

This project has received funding from the European Union's Horizon 2020 research and innovation program under Marie Sklodowska-Curie grants (840290 and 642687); the Ministry of Education, Culture and Science through the Institute of Chemical Immunology (NWO Gravitation program 024.002.009, ICI00024); the Research Center for Functional Molecular Systems (NWO Gravitation program 024.001.035); KU Leuven (grant IDN/20/021); the National Natural Science Foundation of China (32201097); and Excellent Young Scientist Fund of the Natural Science Foundation of Hebei Province (B2022202027). J.V. and H.Y. acknowledge the Research Foundation Flanders (FWO) for their personal fellowships (1186220N and 12A2423N).

AUTHOR CONTRIBUTIONS

All authors contributed to the writing of this review.

DECLARATION OF INTERESTS

The authors declare patents on PIC hydrogels (WO2018/197416 and WO2018/104324, P.H.J.K.) and on PIC immunofilaments (WO2019/154865A1 and WO2020/174041A1, R.H.).

REFERENCES

1. Ugi, I., Werner, B., and Dömling, A. (2003). The Chemistry of Isocyanides, their MultiComponent Reactions and their Libraries. Molecules *8*, 53–66. https://doi.org/10.3390/80100053.

2. Ugi, I., and Meyr, R. (1958). Neue Darstellungsmethode für Isonitrile. Angew. Chem. *70*, 702–703. https://doi.org/10.1002/ange.19580702213.

3. Millich, F. (1972). Polymerization of isocyanides. Chem. Rev. *72*, 101–113. https://doi.org/10.1021/cr60276a001.

4. Ito, Y., Ihara, E., Murakami, M., and Shiro, M. (1990). New living polymerization of 1,2-diisocyanoarenes via (quinoxalinyl)palladium complexes. Synthesis of poly(2,3-quinoxaline). J. Am. Chem. Soc. *112*, 6446–6447. https://doi.org/10.1021/ja00173a070.

5. Onitsuka, K., Joh, T., and Takahashi, S. (1992). Reaction of Heterodinuclear μ-Ethynediyl Complexes Containing Palladium and Platinum: Multiple and Successive Insertion of Isocyanides. Angew. Chem. Int. Ed. Engl. *31*, 851–852. https://doi.org/10.1002/anie.199208511.

6. Onitsuka, K., Yamamoto, M., Mori, T., Takei, F., and Takahashi, S. (2006). Living Polymerization of Bulky Aryl Isocyanide with Arylrhodium Complexes. Organometallics *25*, 1270–1278. https://doi.org/10.1021/om0509692.

7. van Beijnen, J.M., Nolte, R.J.M., Naaktgeboren, A.J., Zwikker, J.W., and Drenth, W. (1983). Helical Configuration of Poly(iminomethy1enes). Synthesis and CD Spectra of Polymers Derived from Optically. Active Isocy anides *16*, 11.

8. Deming, T.J., and Novak, B.M. (1991). Organometallic catalysis in air and water: oxygen-enhanced, nickel-catalyzed polymerizations of isocyanides. Macromolecules *24*, 326–328. https://doi.org/10.1021/ma00001a051.

9. Nolte, R.J.M. (1994). Helical poly(isocyanides). Chem. Soc. Rev. *23*, 11. https://doi.org/10.1039/cs9942300011.

10. Cornelissen, J.J., Rowan, A.E., Nolte, R.J., and Sommerdijk, N.A. (2001). Chiral Architectures from Macromolecular Building Blocks. Chem. Rev. *101*, 4039–4070. https://doi.org/10.1021/cr990126i.

11. Leigh, T., and Fernandez-Trillo, P. (2020). Helical polymers for biological and medical applications. Nat. Rev. Chem *4*, 291–310. https://doi.org/10.1038/s41570-020-0180-5.

12. Huang, J.-T., Sun, J., Euler, W.B., and Rosen, W. (1997). Aggregation kinetics and precipitation phenomena in poly(phenylisocyanide). J. Polym. Sci. Part Polym. Chem. *35*, 439–446. https://doi.org/10.1002/(SICI)1099-0518(199702)35:3<439::AID-POLA6>3.0.CO;2-N.

13. Green, M.M., Gross, R.A., Schilling, F.C., Zero, K., and Crosby, C. (1988). Macromolecular stereochemistry: effect of pendant group structure on the conformational properties of polyisocyanides. Macromolecules *21*, 1839–1846. https://doi.org/10.1021/ma00184a051.

14. Cornelissen, J.J., Donners, J.J., de Gelder, R., Graswinckel, W.S., Metselaar, G.A., Rowan, A.E., Sommerdijk, N.A., and Nolte, R.J. (2001). beta -Helical Polymers from Isocyanopeptides. Science *293*, 676–680. https://doi.org/10.1126/science.1062224.

15. Cornelissen, J.J.L.M., Graswinckel, W.S., Adams, P.J.H.M., Nachtegaal, G.H., Kentgens, A.P.M., Sommerdijk, N.A.J.M., and Nolte, R.J.M. (2001). Synthesis and characterization of polyisocyanides derived from alanine and glycine dipeptides. J. Polym.

Sci. A. Polym. Chem. *39*, 4255–4264. https://doi.org/10.1002/pola.10083.

16. Metselaar, G.A., Adams, P.J.H.M., Nolte, R.J.M., Cornelissen, J.J.L.M., and Rowan, A.E. (2007). Polyisocyanides Derived from Tripeptides of Alanine. Chem. Eur J. *13*, 950–960. https://doi.org/10.1002/chem.200600928.

17. Gerrits, L., Hammink, R., and Kouwer, P.H.J. (2021). Semiflexible polymer scaffolds: an overview of conjugation strategies. Polym. Chem. *12*, 1362–1392. https://doi.org/10.1039/D0PY01662D.

18. Samorí, P., Ecker, C., Gössl, I., de Witte, P.A.J., Cornelissen, J.J.L.M., Metselaar, G.A., Otten, M.B.J., Rowan, A.E., Nolte, R.J.M., and Rabe, J.P. (2002). High Shape Persistence in Single Polymer Chains Rigidified with Lateral Hydrogen Bonded Networks. Macromolecules *35*, 5290–5294. https://doi.org/10.1021/ma011946b.

19. Palermo, V., Schwartz, E., Finlayson, C.E., Liscio, A., Otten, M.B.J., Trapani, S., Müllen, K., Beljonne, D., Friend, R.H., Nolte, R.J.M., et al. (2010). Macromolecular Scaffolding: The Relationship Between Nanoscale Architecture and Function in Multichromophoric Arrays for Organic Electronics. Adv. Mater. *22*, E81–E88. https://doi.org/10.1002/adma.200903672.

20. Schwartz, E., Le Gac, S., Cornelissen, J.J.L.M., Nolte, R.J.M., and Rowan, A.E. (2010). Macromolecular multi-chromophoric scaffolding. Chem. Soc. Rev. *39*, 1576–1599. https://doi.org/10.1039/B922160C.

21. Schwartz, E., Koepf, M., Kitto, H.J., Espelt, M., Nebot-Carda, V.J., De Gelder, R., Nolte, R.J.M., Cornelissen, J.J.L.M., and Rowan, A.E. (2009). Water soluble azido polyisocyanopeptides as functional β-sheet mimics: Water Soluble Azido Polyisocyanopeptides. J. Polym. Sci. A. Polym. Chem. *47*, 4150–4164. https://doi.org/10.1002/pola.23477.

22. Kitto, H.J., Schwartz, E., Nijemeisland, M., Koepf, M., Cornelissen, J.J.L.M., Rowan, A.E., and Nolte, R.J.M. (2008). Post-modification of helical dipeptido polyisocyanides using the 'click' reaction. J. Mater. Chem. *18*, 5615. https://doi.org/10.1039/b811002f.

23. Koepf, M., Kitto, H.J., Schwartz, E., Kouwer, P.H., Nolte, R.J., and Rowan, A.E. (2013). Preparation and characterization of non-linear poly(ethylene glycol) analogs from oligo(ethylene glycol) functionalized polyisocyanopeptides. Eur. Polym. J. *49*, 1510–1522. https://doi.org/10.1016/j.eurpolymj.2013.01.009.

24. Jaspers, M., Dennison, M., Mabesoone, M.F.J., MacKintosh, F.C., Rowan, A.E., and Kouwer, P.H.J. (2014). Ultra-responsive soft matter from strain-stiffening hydrogels. Nat. Commun. *5*, 5808. https://doi.org/10.1038/ncomms6808.

25. Kouwer, P.H.J., Koepf, M., Le Sage, V.A.A., Jaspers, M., van Buul, A.M., Eksteen-Akeroyd, Z.H., Woltinge, T., Schwartz, E., Kitto, H.J., Hoogenboom, R., et al. (2013). Responsive biomimetic networks from polyisocyanopeptide hydrogels. Nature *493*, 651–655. https://doi.org/10.1038/nature11839.

26. Nolte, R.J., and Rowan, A.E. (2016). Bio-Inspired Polymer Chemistry. Tuning the Structure and Properties of Self-Assembled Polymers by Solvent Interactions. Macromol. Symp. *369*, 97–100. https://doi.org/10.1002/masy.201600063.

27. Yuan, H., Xu, J., van Dam, E.P., Giubertoni, G., Rezus, Y.L.A., Hammink, R., Bakker, H.J., Zhan, Y., Rowan, A.E., Xing, C., and Kouwer, P.H.J. (2017). Strategies To Increase the Thermal Stability of Truly Biomimetic Hydrogels: Combining Hydrophobicity and Directed Hydrogen Bonding. Macromolecules *50*, 9058–9065. https://doi.org/10.1021/acs.macromol.7b01832.

28. Zinkevich, T., Venderbosch, B., Jaspers, M., Kouwer, P.H.J., Rowan, A.E., van Eck, E.R.H., and Kentgens, A.P.M. (2016). Solid-state NMR characterization of tri-ethyleneglycol grafted polyisocyanopeptides. Magn. Reson. Chem. *54*, 328–333. https://doi.org/10.1002/mrc.4379.

29. Kouwer, P.H., de Almeida, P., ven den Boomen, O., Eksteen-Akeroyd, Z.H., Hammink, R., Jaspers, M., Kragt, S., Mabesoone, M.F., Nolte, R.J., Rowan, A.E., et al. (2018). Controlling the gelation temperature of biomimetic polyisocyanides. Chin. Chem. Lett. *29*, 281–284. https://doi.org/10.1016/j.cclet.2017.11.002.

30. Thormann, E. (2012). On understanding of the Hofmeister effect: how addition of salt alters the stability of temperature responsive polymers in aqueous solutions. RSC Adv. *2*, 8297–8305. https://doi.org/10.1039/C2RA20164J.

31. Jaspers, M., Rowan, A.E., and Kouwer, P.H.J. (2015). Tuning Hydrogel Mechanics Using the Hofmeister Effect. Adv. Funct. Mater. *25*, 6503–6510. https://doi.org/10.1002/adfm.201502241.

32. Gavrilov, M., Gilbert, E.P., Rowan, A.E., Lauko, J., and Yakubov, G.E. (2020). Structural Insights into the Mechanism of Heat-Set Gel Formation of Polyisocyanopeptide Polymers. Macromol. Rapid Commun. *41*, 2000304. https://doi.org/10.1002/marc.202000304.

33. Grason, G.M., and Bruinsma, R.F. (2007). Chirality and Equilibrium Biopolymer Bundles. Phys. Rev. Lett. *99*, 098101. https://doi.org/10.1103/PhysRevLett.99.098101.

34. Jaspers, M., Pape, A.C.H., Voets, I.K., Rowan, A.E., Portale, G., and Kouwer, P.H.J. (2016). Bundle Formation in Biomimetic Hydrogels. Biomacromolecules *17*, 2642–2649. https://doi.org/10.1021/acs.biomac.6b00703.

35. de Loos, M., Feringa, B.L., and van Esch, J.H. (2005). Design and Application of Self-Assembled Low Molecular Weight Hydrogels. Eur. J. Org. Chem. *2005*, 3615–3631. https://doi.org/10.1002/ejoc.200400723.

36. Gardel, M.L. (2013). Synthetic polymers with biological rigidity. Nature *493*, 619. https://doi.org/10.1038/nature11855.

37. van Dam, E.P., Yuan, H., Kouwer, P.H.J., and Bakker, H.J. (2021). Structure and Dynamics of a Temperature-Sensitive Hydrogel. J. Phys. Chem. B *125*, 8219–8224. https://doi.org/10.1021/acs.jpcb.1c03121.

38. Vandaele, J., Louis, B., Liu, K., Camacho, R., Kouwer, P.H.J., and Rocha, S. (2020). Structural characterization of fibrous synthetic hydrogels using fluorescence microscopy. Soft Matter *16*, 4210–4219. https://doi.org/10.1039/C9SM01828J.

39. Ma, C., Liu, K., Li, Q., Xiong, Y., Xu, C., Zhang, W., Ruan, C., Li, X., and Lei, X. (2022). Synthetic Extracellular Matrices for 3D Culture of Schwann Cells, Hepatocytes, and HUVECs. Bioengineering *9*, 453. https://doi.org/10.3390/bioengineering9090453.

40. Stojkov, G., Niyazov, Z., Picchioni, F., and Bose, R.K. (2021). Relationship between Structure and Rheology of Hydrogels for Various Applications. Gels *7*, 255. https://doi.org/10.3390/gels7040255.

41. Krieg, M., Fläschner, G., Alsteens, D., Gaub, B.M., Roos, W.H., Wuite, G.J.L., Gaub, H.E., Gerber, C., Dufrêne, Y.F., and Müller, D.J. (2018). Atomic force microscopy-based mechanobiology. Nat. Rev. Phys. *1*, 41–57. https://doi.org/10.1038/s42254-018-0001-7.

42. Joshi, J., Homburg, S.V., and Ehrmann, A. (2022). Atomic Force Microscopy (AFM) on Biopolymers and Hydrogels for Biotechnological Applications—Possibilities and Limits. Polymers *14*, 1267. https://doi.org/10.3390/polym14061267.

43. Liang, W., Shi, H., Yang, X., Wang, J., Yang, W., Zhang, H., and Liu, L. (2020). Recent advances in AFM-based biological characterization and applications at multiple levels. Soft Matter *16*, 8962–8984. https://doi.org/10.1039/D0SM01106A.

44. Norman, M.D.A., Ferreira, S.A., Jowett, G.M., Bozec, L., and Gentleman, E. (2021). Measuring the Elastic Modulus of Soft Culture Surfaces and Three-Dimensional Hydrogels Using Atomic Force Microscopy. Nature Protocols *16*, 2418. https://doi.org/10.1038/s41596-021-00495-4.

45. Brosey, C.A., and Tainer, J.A. (2019). Evolving SAXS versatility: solution X-ray scattering for macromolecular architecture, functional landscapes, and integrative structural biology. Curr. Opin. Struct. Biol. *58*, 197–213. https://doi.org/10.1016/j.sbi.2019.04.004.

46. Goldstein, J.I., Newbury, D.E., Michael, J.R., Ritchie, N.W.M., Scott, J.H.J., and Joy, D.C. (2018). Scanning Electron Microscopy and X-Ray Microanalysis (Springer New York). https://doi.org/10.1007/978-1-4939-6676-9.

47. Cheng, Y., Grigorieff, N., Penczek, P.A., and Walz, T. (2015). A Primer to Single-Particle Cryo-Electron Microscopy. Cell *161*, 438–449. https://doi.org/10.1016/j.cell.2015.03.050.

48. Frank, J. (2017). Advances in the field of single-particle cryo-electron microscopy over the last decade. Nat. Protoc. *12*, 209–212. https://doi.org/10.1038/nprot.2017.004.

49. Kaberova, Z., Karpushkin, E., Nevoralová, M., Vetrík, M., Šlouf, M., and Dušková-Smrčková, M. (2020). Microscopic Structure of Swollen Hydrogels by Scanning Electron and Light Microscopies: Artifacts and Reality. Polymers *12*, 578. https://doi.org/10.3390/polym12030578.

50. Herman, B. (2020). Fluorescence Microscopy (Garland Science). https://doi.org/10.1201/9781003077060.

51. Lichtman, J.W., and Conchello, J.-A. (2005). Fluorescence microscopy. Nat. Methods *2*, 910–919. https://doi.org/10.1038/nmeth817.

52. Vangindertael, J., Camacho, R., Sempels, W., Mizuno, H., Dedecker, P., and Janssen, K.P.F. (2018). An introduction to optical super-resolution microscopy for the adventurous biologist. Methods Appl. Fluoresc. *6*, 022003. https://doi.org/10.1088/2050-6120/aaae0c.

53. Lelek, M., Gyparaki, M.T., Beliu, G., Schueder, F., Griffié, J., Manley, S., Jungmann, R., Sauer, M., Lakadamyali, M., and Zimmer, C. (2021). Single-molecule localization microscopy. Nat. Rev. Methods Primers *1*, 39–27. https://doi.org/10.1038/s43586-021-00038-x.

54. Ollier, R.C., Xiang, Y., Yacovelli, A.M., and Webber, M.J. (2023). Biomimetic strain-stiffening in fully synthetic dynamic-covalent hydrogel networks. Chem. Sci. *14*, 4796–4805. https://doi.org/10.1039/D3SC00011G.

55. Liu, Y., Lin, S.-H., Chuang, W.-T., Dai, N.-T., and Hsu, S.H. (2022). Biomimetic Strain-Stiffening in Chitosan Self-Healing Hydrogels. ACS Appl. Mater. Interfaces *14*, 16032–16046. https://doi.org/10.1021/acsami.2c01720.

56. Wang, Y., Xu, Z., Lovrak, M., le Sage, V.A.A., Zhang, K., Guo, X., Eelkema, R., Mendes, E., and van Esch, J.H. (2020). Biomimetic Strain-Stiffening Self-Assembled Hydrogels. Angew. Chem. *132*, 4860–4864. https://doi.org/10.1002/ange.201911364.

57. Wang, W., Xiang, L., Diaz-Dussan, D., Zhang, J., Yang, W., Gong, L., Chen, J., Narain, R., and Zeng, H. (2020). Dynamic Flexible Hydrogel Network with Biological Tissue-like Self-Protective Functions. Chem. Mater. *32*, 10545–10555. https://doi.org/10.1021/acs.chemmater.0c03526.

58. Xu, J., Jiang, Y., and Gao, L. (2023). Synthetic strain-stiffening hydrogels towards mechanical adaptability. J. Mater. Chem. B *11*, 221–243. https://doi.org/10.1039/D2TB01743A.

59. Broedersz, C., and MacKintosh, F. (2014). Modeling semiflexible polymer networks. Rev. Mod. Phys. *86*, 995–1036. https://doi.org/10.1103/RevModPhys.86.995.

60. Dennison, M., Jaspers, M., Kouwer, P.H.J., Storm, C., Rowan, A.E., and MacKintosh, F.C. (2016). Critical behaviour in the nonlinear elastic response of hydrogels. Soft Matter *12*, 6995–7004. https://doi.org/10.1039/C6SM01033D.

61. Chaudhuri, O., Cooper-White, J., Janmey, P.A., Mooney, D.J., and Shenoy, V.B. (2020). Effects of extracellular matrix viscoelasticity on cellular behaviour. Nature *584*, 535–546. https://doi.org/10.1038/s41586-020-2612-2.

62. Liu, K., Wiendels, M., Yuan, H., Ruan, C., and Kouwer, P.H.J. (2022). Cell-matrix reciprocity in 3D culture models with nonlinear elasticity. Bioact. Mater. *9*, 316–331. https://doi.org/10.1016/j.bioactmat.2021.08.002.

63. Das, R.K., Gocheva, V., Hammink, R., Zouani, O.F., and Rowan, A.E. (2016). Stress-stiffening-mediated stem-cell commitment switch in soft responsive hydrogels. Nat. Mater. *15*, 318–325. https://doi.org/10.1038/nmat4483.

64. Broedersz, C.P., Sheinman, M., and MacKintosh, F.C. (2012). Filament-Length-Controlled Elasticity in 3D Fiber Networks. Phys. Rev. Lett. *108*, 078102. https://doi.org/10.1103/PhysRevLett.108.078102.

65. Yuan, H., Liu, K., Cóndor, M., Barrasa-Fano, J., Louis, B., Vandaele, J., de Almeida, P., Coucke, Q., Chen, W., Oosterwijk, E., et al. (2023). Synthetic fibrous hydrogels as a platform to decipher cell–matrix mechanical interactions. Proc. Natl. Acad. Sci. USA *120*, e2216934120. https://doi.org/10.1073/pnas.2216934120.

66. Jansen, K.A., Bacabac, R.G., Piechocka, I.K., and Koenderink, G.H. (2013). Cells Actively Stiffen Fibrin Networks by Generating Contractile Stress. Biophys. J. *105*, 2240–2251. https://doi.org/10.1016/j.bpj.2013.10.008.

67. Al-Dirini, R.M.A., Reed, M.P., and Thewlis, D. (2015). Deformation of the gluteal soft tissues during sitting. Clin. Biomech. *30*, 662–668. https://doi.org/10.1016/j.clinbiomech.2015.05.008.

68. de Almeida, P., Janmey, P.A., and Kouwer, P.H.J. (2021). Fibrous Hydrogels under Multi-Axial Deformation: Persistence Length as the Main Determinant of Compression Softening. Adv. Funct. Mater. *31*, 2010527. https://doi.org/10.1002/adfm.202010527.

69. Janmey, P.A., Georges, P.C., and Hvidt, S. (2007). Basic rheology for biologists. Methods Cell Biol. *83*, 3–27. https://doi.org/10.1016/S0091-679X(07)83001-9.

70. Broedersz, C.P., Kasza, K.E., Jawerth, L.M., Münster, S., Weitz, D.A., and MacKintosh, F.C. (2010). Measurement of nonlinear rheology of cross-linked biopolymer gels. Soft Matter *6*, 4120–4127. https://doi.org/10.1039/C0SM00285B.

71. Grolman, J.M., Weinand, P., and Mooney, D.J. (2020). Extracellular matrix plasticity as a driver of cell spreading. Proc. Natl. Acad. Sci. USA *117*, 25999–26007. https://doi.org/10.1073/pnas.2008801117.

72. Schoenmakers, D.C., Rowan, A.E., and Kouwer, P.H.J. (2018). Crosslinking of fibrous hydrogels. Nat. Commun. *9*, 2172. https://doi.org/10.1038/s41467-018-04508-x.

73. Chen, W., and Kouwer, P.H.J. (2021). Combining Mechanical Tuneability with Function: Biomimetic Fibrous Hydrogels with Nanoparticle Crosslinkers. Adv. Funct. Mater. *31*, 2105713. https://doi.org/10.1002/adfm.202105713.

74. Chen, W., Kumari, J., Yuan, H., Yang, F., and Kouwer, P.H.J. (2022). Toward Tissue-Like Material Properties: Inducing In Situ Adaptive Behavior in Fibrous Hydrogels. Adv. Mater. *34*, 2202057. https://doi.org/10.1002/adma.202202057.

75. Schoenmakers, D.C., Schoonen, L., Rutten, M.G.T.A., Nolte, R.J.M., Rowan, A.E., van Hest, J.C.M., and Kouwer, P.H.J. (2018). Virus-like particles as crosslinkers in fibrous biomimetic hydrogels: approaches towards capsid rupture and gel repair. Soft Matter *14*, 1442–1448. https://doi.org/10.1039/C7SM02320K.

76. Deshpande, S.R., Hammink, R., Nelissen, F.H.T., Rowan, A.E., and Heus, H.A. (2017). Biomimetic Stress Sensitive Hydrogel Controlled by DNA Nanoswitches. Biomacromolecules *18*, 3310–3317. https://doi.org/10.1021/acs.biomac.7b00964.

77. de Almeida, P., Jaspers, M., Vaessen, S., Tagit, O., Portale, G., Rowan, A.E., and Kouwer, P.H.J. (2019). Cytoskeletal stiffening in synthetic hydrogels. Nat. Commun. *10*, 609. https://doi.org/10.1038/s41467-019-08569-4.

78. Chen, W., Zhang, Y., Kumari, J., Engelkamp, H., and Kouwer, P.H.J. (2021). Magnetic Stiffening in 3D Cell Culture Matrices. Nano Lett. *21*, 6740–6747. https://doi.org/10.1021/acs.nanolett.1c00371.

79. Grad, E.M., Tunn, I., Voerman, D., de Léon, A.S., Hammink, R., and Blank, K.G. (2020). Influence of Network Topology on the Viscoelastic Properties of Dynamically Crosslinked Hydrogels. Front. Chem. *8*, 536. https://doi.org/10.3389/fchem.2020.00536.

80. Deshpande, S.R., Hammink, R., Das, R.K., Nelissen, F.H.T., Blank, K.G., Rowan, A.E., and Heus, H.A. (2016). DNA-Responsive Polyisocyanopeptide Hydrogels with Stress-Stiffening Capacity. Adv. Funct. Mater. *26*, 9075–9082. https://doi.org/10.1002/adfm.201602461.

81. Bruekers, S.M.C., Jaspers, M., Hendriks, J.M.A., Kurniawan, N.A., Koenderink, G.H., Kouwer, P.H.J., Rowan, A.E., and T S Huck, W. (2016). Fibrin-fiber architecture influences cell spreading and differentiation. Cell Adh. Migr. *10*, 495–504. https://doi.org/10.1080/19336918.2016.1151607.

82. Jaspers, M., Vaessen, S.L., van Schayik, P., Voerman, D., Rowan, A.E., and Kouwer, P.H.J. (2017). Nonlinear mechanics of hybrid polymer networks that mimic the complex mechanical environment of cells. Nat. Commun. *8*, 15478. https://doi.org/10.1038/ncomms15478.

83. Chen, W., Zhang, Z., and Kouwer, P.H.J. (2022). Magnetically Driven Hierarchical Alignment in Biomimetic Fibrous Hydrogels. Small *18*, 2203033. https://doi.org/10.1002/smll.202203033.

84. Zhang, Y., Zegers, M.M.P., Nagelkerke, A., Rowan, A.E., Span, P.N., and Kouwer, P.H.J. (2021). Tunable Hybrid Matrices Drive Epithelial Morphogenesis and YAP Translocation. Adv. Sci. *8*, 2003380. https://doi.org/10.1002/advs.202003380.

85. Klimek, K., and Ginalska, G. (2020). Proteins and Peptides as Important Modifiers of the Polymer Scaffolds for Tissue Engineering Applications—A Review. Polymers *12*, 844. https://doi.org/10.3390/polym12040844.

86. Van Velthoven, M.J.J., Gudde, A.N., Enting, H., Hammink, R., Roovers, J., Guler, Z., Oosterwijk, E., and Kouwer, P.H.J. (2023). Potential of Estradiol-Functionalized Polyisocyanide Hydrogels for Stimulating Tissue Regeneration of the Pelvic Floor. Adv. Ther. *7*, 2300199. https://doi.org/10.1002/adtp.202300199.

87. Van Velthoven, M.J.J., Gudde, A.N., Arendsen, E., Roovers, J.P., Guler, Z., Oosterwijk, E., and Kouwer, P.H.J. (2023). Growth Factor Immobilization to Synthetic Hydrogels: Bioactive bFGF-Functionalized Polyisocyanide Hydrogels. Adv. Healthc. Mater. *12*, 2301109. https://doi.org/10.1002/adhm.202301109.

88. Huettner, N., Dargaville, T.R., and Forget, A. (2018). Discovering Cell-Adhesion Peptides in Tissue Engineering: Beyond RGD. Trends Biotechnol. *36*, 372–383. https://doi.org/10.1016/j.tibtech.2018.01.008.

89. Liu, K., Mihaila, S.M., Rowan, A., Oosterwijk, E., and Kouwer, P.H.J. (2019). Synthetic Extracellular Matrices with Nonlinear Elasticity Regulate Cellular Organization. Biomacromolecules *20*, 826–834. https://doi.org/10.1021/acs.biomac.8b01445.

90. Zimoch, J., Padial, J.S., Klar, A.S., Vallmajo-Martin, Q., Meuli, M., Biedermann, T., Wilson, C.J., Rowan, A., and Reichmann, E. (2018). Polyisocyanopeptide hydrogels: A novel thermo-responsive hydrogel supporting pre-vascularization and the development of organotypic structures. Acta Biomater. *70*, 129–139. https://doi.org/10.1016/j.actbio.2018.01.042.

91. Zhang, Y., Tang, C., Span, P.N., Rowan, A.E., Aalders, T.W., Schalken, J.A., Adema, G.J., Kouwer, P.H.J., Zegers, M.M.P., and Ansems, M. (2020). Polyisocyanide Hydrogels as a Tunable Platform for Mammary Gland Organoid Formation. Adv. Sci. *7*, 2001797. https://doi.org/10.1002/advs.202001797.

92. Gudde, A.N., van Velthoven, M.J.J., Roovers, J.-P.W.R., Kouwer, P.H.J., and Guler, Z. (2022). Polyisocyanides as a substrate to trigger vaginal fibroblast functioning in an in vitro model for prolapse repair. Biomater. Adv. *141*, 213104. https://doi.org/10.1016/j.bioadv.2022.213104.

93. Zhang, Z., Chen, W., Tiemessen, D.M., Oosterwijk, E., and Kouwer, P.H.J. (2022). A Temperature-Based Easy-Separable (TempEasy) 3D Hydrogel Coculture System. Adv. Healthc. Mater. *11*, 2102389. https://doi.org/10.1002/adhm.202102389.

94. Kumari, J., Wagener, F.A.D.T.G., and Kouwer, P.H.J. (2022). Novel Synthetic Polymer-Based 3D Contraction Assay: A Versatile Preclinical Research Platform for Fibrosis. ACS Appl. Mater. Interfaces *14*, 19212–19225. https://doi.org/10.1021/acsami.2c02549.

95. Trappmann, B., Gautrot, J.E., Connelly, J.T., Strange, D.G.T., Li, Y., Oyen, M.L., Cohen Stuart, M.A., Boehm, H., Li, B., Vogel, V., et al. (2012). Extracellular-matrix tethering regulates stem-cell fate. Nat. Mater. *11*, 642–649. https://doi.org/10.1038/nmat3339.

96. Engler, A.J., Sen, S., Sweeney, H.L., and Discher, D.E. (2006). Matrix Elasticity Directs Stem Cell Lineage Specification. Cell *126*, 677–689. https://doi.org/10.1016/j.cell.2006.06.044.

97. Narasimhan, B.N., Horrocks, M.S., and Malmström, J. (2021). Hydrogels with Tunable Physical Cues and Their Emerging Roles in Studies of Cellular Mechanotransduction. Adv. NanoBiomed Res. *1*, 2100059. https://doi.org/10.1002/anbr.202100059.

98. Liu, K., Vandaele, J., Bernhagen, D., Erp, M. van, Oosterwijk, E., Timmerman, P., Rocha, S., and Kouwer, P.H.J. (2022). Rapid stem cell spreading induced by high affinity α5β1 integrin-selective bicyclic RGD peptide in biomimetic hydrogels. Preprint at bioRxiv. https://doi.org/10.1101/2022.02.01.478177.

99. Liu, K., Veenendaal, T., Wiendels, M., Ruiz-Zapata, A.M., van Laar, J., Kyranas, R., Enting, H., van Cranenbroek, B., Koenen, H.J.P.M., Mihaila, S.M., et al. (2020). Synthetic Extracellular Matrices as a Toolbox to Tune Stem Cell Secretome. ACS Appl. Mater. Interfaces *12*, 56723–56730. https://doi.org/10.1021/acsami.0c16208.

100. Wu, P.-H., Aroush, D.R.-B., Asnacios, A., Chen, W.-C., Dokukin, M.E., Doss, B.L., Durand-Smet, P., Ekpenyong, A., Guck, J., Guz, N.V., et al. (2018). A comparison of methods to assess cell mechanical properties. Nat. Methods *15*, 491–498. https://doi.org/10.1038/s41592-018-0015-1.

101. Kechagia, J.Z., Ivaska, J., and Roca-Cusachs, P. (2019). Integrins as biomechanical sensors of the microenvironment. Nat. Rev. Mol. Cell Biol. *20*, 457–473. https://doi.org/10.1038/s41580-019-0134-2.

102. van Helvert, S., Storm, C., and Friedl, P. (2018). Mechanoreciprocity in cell migration. Nat. Cell Biol. *20*, 8–20. https://doi.org/10.1038/s41556-017-0012-0.

103. Baker, B.M., Trappmann, B., Wang, W.Y., Sakar, M.S., Kim, I.L., Shenoy, V.B., Burdick, J.A., and Chen, C.S. (2015). Cell-mediated fibre recruitment drives extracellular matrix mechanosensing in engineered fibrillar microenvironments. Nat. Mater. *14*, 1262–1268. https://doi.org/10.1038/nmat4444.

104. Liu, J., Qu, S., Suo, Z., and Yang, W. (2020). Functional Hydrogel Coatings. Natl. Sci. Rev. *8*, nwaa254. https://doi.org/10.1093/nsr/nwaa254.

105. Yang, R., Wang, X., Yan, S., Dong, A., Luan, S., and Yin, J. (2021). Advances in design and biomedical application of hierarchical polymer brushes. Prog. Polym. Sci. *118*, 101409. https://doi.org/10.1016/j.progpolymsci.2021.101409.

106. Murad Bhayo, A., Yang, Y., and He, X. (2022). Polymer brushes: Synthesis, characterization, properties and applications. Prog. Mater. Sci. *130*, 101000. https://doi.org/10.1016/j.pmatsci.2022.101000.

107. Tavakoli, J., and Tang, Y. (2017). Hydrogel Based Sensors for Biomedical Applications: An Updated Review. Polymers *9*, 364. https://doi.org/10.3390/polym9080364.

108. Kotlarek, D., Liu, K., Quilis, N.G., Bernhagen, D., Timmerman, P., Kouwer, P., and Dostalek, J. (2021). Thin-Film Polyisocyanide-Based Hydrogels for Affinity Biosensors. J. Phys. Chem. C *125*, 12960–12967. https://doi.org/10.1021/acs.jpcc.1c02489.

109. Chimene, D., Kaunas, R., and Gaharwar, A.K. (2020). Hydrogel Bioink Reinforcement for Additive Manufacturing: A Focused Review of Emerging Strategies. Adv. Mater. *32*, 1902026. https://doi.org/10.1002/adma.201902026.

110. Ruan, C., Qu, H., Gao, C., Liu, K., Fu, H., Liu, Z., Kouwer, P., and Han, Z. (2023). Gradient matters via filament diameter-adjustable 3D printing. In Review. https://doi.org/10.21203/rs.3.rs-3393829/v1.

111. Celikkin, N., Simó Padial, J., Costantini, M., Hendrikse, H., Cohn, R., Wilson, C.J., Rowan, A.E., and Święszkowski, W. (2018). 3D Printing of Thermoresponsive Polyisocyanide (PIC) Hydrogels as Bioink and Fugitive Material for Tissue Engineering. Polymers *10*, 555. https://doi.org/10.3390/polym10050555.

112. Lee, S.C., Gillispie, G., Prim, P., and Lee, S.J. (2020). Physical and Chemical Factors Influencing the Printability of Hydrogel-based Extrusion Bioinks. Chem. Rev. *120*, 10834–10886. https://doi.org/10.1021/acs.chemrev.0c00015.

113. Sies, H., Belousov, V.V., Chandel, N.S., Davies, M.J., Jones, D.P., Mann, G.E., Murphy, M.P., Yamamoto, M., and Winterbourn, C. (2022). Defining roles of specific reactive oxygen species (ROS) in cell biology and physiology. Nat. Rev. Mol. Cell Biol. *23*, 499–515. https://doi.org/10.1038/s41580-022-00456-z.

114. Guo, J., Xing, C., Yuan, H., Chai, R., and Zhan, Y. (2019). Oligo (p-Phenylene Vinylene)/Polyisocyanopeptide Biomimetic Composite Hydrogel-Based Three-Dimensional Cell Culture System for Anticancer and Antibacterial Therapeutics. ACS Appl. Bio Mater. *2*, 2520–2527. https://doi.org/10.1021/acsabm.9b00217.

115. Du, C., Gao, D., Gao, M., Yuan, H., Liu, X., Wang, B., and Xing, C. (2021). Property Regulation of Conjugated Oligoelectrolytes with Polyisocyanide to Achieve Efficient Photodynamic Antibacterial Biomimetic Hydrogels. ACS Appl. Mater. Interfaces *13*, 27955–27962. https://doi.org/10.1021/acsami.1c06659.

116. Yuan, H., Zhan, Y., Rowan, A.E., Xing, C., and Kouwer, P.H.J. (2020). Biomimetic Networks with Enhanced Photodynamic Antimicrobial Activity from Conjugated Polythiophene/Polyisocyanide Hybrid Hydrogels. Angew. Chem. Int. Ed. *59*, 2720–2724. https://doi.org/10.1002/anie.201910979.

117. Cui, Q., Yuan, H., Bao, X., Ma, G., Wu, M., and Xing, C. (2020). Synergistic Photodynamic and Photothermal Antibacterial Therapy Based on a Conjugated Polymer Nanoparticle-Doped Hydrogel. ACS Appl. Bio Mater. *3*, 4436–4443. https://doi.org/10.1021/acsabm.0c00423.

118. Wang, B., Wang, J., Shao, J., Kouwer, P.H.J., Bronkhorst, E.M., Jansen, J.A., Walboomers, X.F., and Yang, F. (2020). A tunable and injectable local drug delivery system for personalized periodontal application. J. Control. Release *324*, 134–145. https://doi.org/10.1016/j.jconrel.2020.05.004.

119. Wang, B., Booij-Vrieling, H.E., Bronkhorst, E.M., Shao, J., Kouwer, P.H.J., Jansen, J.A., Walboomers, X.F., and Yang, F. (2020). Antimicrobial and anti-inflammatory thermo-reversible hydrogel for periodontal delivery. Acta Biomater. *116*, 259–267. https://doi.org/10.1016/j.actbio.2020.09.018.

120. Veld, R.C. op 't, Joosten, L., van den Boomen, O.I., Boerman, O.C., Kouwer, P., Middelkoop, E., Rowan, A.E., Jansen, J.A., Walboomers,

X.F., and Wagener, F.A.D.T.G. (2019). Monitoring 111In-labelled polyisocyanopeptide (PIC) hydrogel wound dressings in full-thickness wounds. Biomater. Sci. *7*, 3041–3050. https://doi.org/10.1039/C9BM00661C.

121. op 't Veld, R.C., van den Boomen, O.I., Lundvig, D.M.S., Bronkhorst, E.M., Kouwer, P.H.J., Jansen, J.A., Middelkoop, E., Von den Hoff, J.W., Rowan, A.E., and Wagener, F.A.D.T.G. (2018). Thermosensitive biomimetic polyisocyanopeptide hydrogels may facilitate wound repair. Biomaterials *181*, 392–401. https://doi.org/10.1016/j.biomaterials.2018.07.038.

122. Aisenbrey, E.A., and Murphy, W.L. (2020). Synthetic alternatives to Matrigel. Nat. Rev. Mater. *5*, 539–551. https://doi.org/10.1038/s41578-020-0199-8.

123. Kleinman, H.K., and Martin, G.R. (2005). Matrigel: Basement membrane matrix with biological activity. Semin. Cancer Biol. *15*, 378–386. https://doi.org/10.1016/j.semcancer.2005.05.004.

124. Vukicevic, S., Kleinman, H.K., Luyten, F.P., Roberts, A.B., Roche, N.S., and Reddi, A.H. (1992). Identification of multiple active growth factors in basement membrane matrigel suggests caution in interpretation of cellular activity related to extracellular matrix components. Exp. Cell Res. *202*, 1–8. https://doi.org/10.1016/0014-4827(92)90397-Q.

125. Talbot, N.C., and Caperna, T.J. (2015). Proteome array identification of bioactive soluble proteins/peptides in Matrigel: relevance to stem cell responses. Cytotechnology *67*, 873–883. https://doi.org/10.1007/s10616-014-9727-y.

126. Hughes, C.S., Postovit, L.M., and Lajoie, G.A. (2010). Matrigel: A complex protein mixture required for optimal growth of cell culture. Proteomics *10*, 1886–1890. https://doi.org/10.1002/pmic.200900758.

127. Worthington, P., Pochan, D.J., and Langhans, S.A. (2015). Peptide Hydrogels – Versatile Matrices for 3D Cell Culture in Cancer Medicine. Front. Oncol. *5*, 92.

128. Rüdiger, D., Kick, K., Goychuk, A., Vollmar, A.M., Frey, E., and Zahler, S. (2020). Cell-Based Strain Remodeling of a Nonfibrous Matrix as an Organizing Principle for Vasculogenesis. Cell Rep. *32*, 108015. https://doi.org/10.1016/j.celrep.2020.108015.

129. Miller, R.T. (2017). Mechanical properties of basement membrane in health and disease. Matrix Biol. *57–58*, 366–373. https://doi.org/10.1016/j.matbio.2016.07.001.

130. Soofi, S.S., Last, J.A., Liliensiek, S.J., Nealey, P.F., and Murphy, C.J. (2009). The elastic modulus of Matrigel™ as determined by atomic force microscopy. J. Struct. Biol. *167*, 216–219. https://doi.org/10.1016/j.jsb.2009.05.005.

131. Sterilization of Hydrogels for Biomedical Applications: A Review - Galante - 2018 - Journal of Biomedical Materials Research Part B: Applied Biomaterials - Wiley Online Library https://onlinelibrary.wiley.com/doi/10.1002/jbm.b.34048.

132. Op 't Veld, R.C., Eerden, M., Wagener, F.A.D.T.G., Kouwer, P.H.J., Jansen, J.A., and Walboomers, X.F. (2020). Polyisocyanopeptide Hydrogels Are Effectively Sterilized Using Supercritical Carbon Dioxide. Tissue Eng. Part C Methods *26*, 132–141. https://doi.org/10.1089/ten.tec.2019.0305.

133. Eggermont, L.J., Paulis, L.E., Tel, J., and Figdor, C.G. (2014). Towards efficient cancer immunotherapy: advances in developing artificial antigen-presenting cells. Trends Biotechnol. *32*, 456–465. https://doi.org/10.1016/j.tibtech.2014.06.007.

134. Cabeza-Cabrerizo, M., Cardoso, A., Minutti, C.M., Pereira da Costa, M., and Reis e Sousa, C. (2021). Dendritic Cells Revisited. Annu. Rev. Immunol. *39*, 131–166. https://doi.org/10.1146/annurev-immunol-061020-053707.

135. Kim, J.V., Latouche, J.-B., Rivière, I., and Sadelain, M. (2004). The ABCs of artificial antigen presentation. Nat. Biotechnol. *22*, 403–410. https://doi.org/10.1038/nbt955.

136. Wang, X., and Rivière, I. (2016). Clinical manufacturing of CAR T cells: foundation of a promising therapy. Mol. Ther. Oncolytics *3*, 16015. https://doi.org/10.1038/mto.2016.15.

137. Butler, M.O., Lee, J.-S., Ansén, S., Neuberg, D., Hodi, F.S., Murray, A.P., Drury, L., Berezovskaya, A., Mulligan, R.C., Nadler, L.M., and Hirano, N. (2007). Long-Lived Antitumor CD8+ Lymphocytes for Adoptive Therapy Generated Using an Artificial Antigen-Presenting Cell. Clin. Cancer Res. *13*, 1857–1867. https://doi.org/10.1158/1078-0432.CCR-06-1905.

138. Steenblock, E.R., Wrzesinski, S.H., Flavell, R.A., and Fahmy, T.M. (2009). Antigen presentation on artificial acellular substrates: modular systems for flexible, adaptable immunotherapy. Expert Opin. Biol. Ther. *9*, 451–464. https://doi.org/10.1517/14712590902849216.

139. Mandal, S., Eksteen-Akeroyd, Z.H., Jacobs, M.J., Hammink, R., Koepf, M., Lambeck, A.J.A., van Hest, J.C.M., Wilson, C.J., Blank, K., Figdor, C.G., and Rowan, A.E. (2013). Therapeutic nanoworms: towards novel synthetic dendritic cells for immunotherapy. Chem. Sci. *4*, 4168–4174. https://doi.org/10.1039/C3SC51399H.

140. Eggermont, L.J., Hammink, R., Blank, K.G., Rowan, A.E., Tel, J., and Figdor, C.G. (2018). Cytokine-Functionalized Synthetic Dendritic Cells for T Cell Targeted Immunotherapies. Adv. Ther. *1*, 1800021. https://doi.org/10.1002/adtp.201800021.

141. Hammink, R., Eggermont, L.J., Zisis, T., Tel, J., Figdor, C.G., Rowan, A.E., and Blank, K.G. (2017). Affinity-Based Purification of Polyisocyanopeptide Bioconjugates. Bioconjug. Chem. *28*, 2560–2568. https://doi.org/10.1021/acs.bioconjchem.7b00398.

142. Hammink, R., Mandal, S., Eggermont, L.J., Nooteboom, M., Willems, P.H.G.M., Tel, J., Rowan, A.E., Figdor, C.G., and Blank, K.G. (2017). Controlling T-Cell Activation with Synthetic Dendritic Cells Using the Multivalency Effect. ACS Omega *2*, 937–945. https://doi.org/10.1021/acsomega.6b00436.

143. Mandal, S., Hammink, R., Tel, J., Eksteen-Akeroyd, Z.H., Rowan, A.E., Blank, K., and Figdor, C.G. (2015). Polymer-Based Synthetic Dendritic Cells for Tailoring Robust and Multifunctional T Cell Responses. ACS Chem. Biol. *10*, 485–492. https://doi.org/10.1021/cb500455g.

144. Mempel, T.R., Henrickson, S.E., and von Andrian, U.H. (2004). T-cell priming by dendritic cells in lymph nodes occurs in three distinct phases. Nature *427*, 154–159. https://doi.org/10.1038/nature02238.

145. Schluck, M., Eggermont, L.J., Weiden, J., Popelier, C., Weiss, L., Pilzecker, B., Kolder, S., Heinemans, A., Rodriguez Mogeda, C., Verdoes, M., et al. Dictating Phenotype, Function, and Fate of Human T Cells with Co-stimulatory Antibodies Presented by Filamentous Immune Cell Mimics. Adv. Ther. n/a, 5 2200019. 10.1002/adtp.202200019.

146. Weiss, L., Weiden, J., Dölen, Y., Grad, E.M., van Dinther, E.A.W., Schluck, M., Eggermont, L.J., van Mierlo, G., Gileadi, U., Bartoló-Ibars, A., et al. (2023). Direct In Vivo Activation of T Cells with Nanosized Immunofilaments Inhibits Tumor Growth and Metastasis. ACS Nano *17*, 12101–12117. https://doi.org/10.1021/acsnano.2c11884.

147. Voerman, D., Schluck, M., Weiden, J., Joosten, B., Eggermont, L.J., van den Eijnde, T., Ignacio, B., Cambi, A., Figdor, C.G., Kouwer, P.H.J., et al. (2019). Synthetic Semiflexible and Bioactive Brushes. Biomacromolecules *20*, 2587–2597. https://doi.org/10.1021/acs.biomac.9b00385.

148. Hammink, R., Weiden, J., Voerman, D., Popelier, C., Eggermont, L.J., Schluck, M., Figdor, C.G., and Verdoes, M. (2021). Semiflexible Immunobrushes Induce Enhanced T Cell Activation and Expansion. ACS Appl. Mater. Interfaces *13*, 16007–16018. https://doi.org/10.1021/acsami.0c21994.

149. Zhang, Z., Tang, C., Hammink, R., Nelissen, F.H.T., Heus, H.A., and Kouwer, P.H.J.H. (2021). Multivalent Sgc8c-aptamer decorated polymer scaffolds for leukemia targeting. Chem. Commun. *57*, 2744–2747. https://doi.org/10.1039/D0CC08205H.

150. Kristyanto, H., Holborough-Kerkvliet, M.D., Lelieveldt, L., Bartels, Y., Hammink, R., Van Schie, K.A.J., Toes, R.E.M., Bonger, K.M., and Scherer, H.U. (2022). Multifunctional, Multivalent PIC Polymer Scaffolds for Targeting Antigen-Specific, Autoreactive B Cells. ACS Biomater. Sci. Eng. *8*, 1486–1493. https://doi.org/10.1021/acsbiomaterials.1c01395.

151. Storm, C., Pastore, J.J., MacKintosh, F.C., Lubensky, T.C., and Janmey, P.A. (2005). Nonlinear elasticity in biological gels. Nature *435*, 191–194. https://doi.org/10.1038/nature03521.

152. Alisafaei, F., Chen, X., Leahy, T., Janmey, P.A., and Shenoy, V.B. (2021). Long-range mechanical signaling in biological systems. Soft Matter *17*, 241–253. https://doi.org/10.1039/D0SM01442G.